Chapter 4

Fast Smoothing of Superficial Respiration Artifacts in CT-Volumes

4.1 Introduction

During CT data acquisition the normal breathing process, internal organ movements, and patient global movements might introduce motion artifacts in the acquired raw data. This motion may be in three dimensions and generally result in artifacts that appear as streaks or distorted semi-transparent structures in the general vicinity of the motion. Using conventional techniques for data acquisition the diagnostic information are significantly reduced due to the motion blurring. Therefore in diagnostic imaging examinations that include the chest or the upper abdomen, the patient must also hold the breath, and it may be necessary for multi-slice studies to be acquired in several single-breath-hold sections. In diagnostic imaging there are several perceptions proposed to overcome the motion blurring on the images [Ritch96], [RitmA90], [RitmB90].

In contrast to diagnostic imaging motion artifacts in CT images have a completely different impact and appreciation in RTP [Lange01]. During tumour irradiation the patient might be immobilized but the breathing process continues normally and freely. In radiation therapy we cannot demand from patient to regulate breathing as can be done in diagnostic imaging during data acquisition. Main reason for that is that the irradiation process lasts more than one minute and therefore is it not possible for the patient to stop breathing and in addition to that some of the patients are having severe respiration disruptions. Irradiation of patient with gating has been proposed as alternative, but these techniques still belong to the non-standardized methods [Wong99]. Considering the above it would be more accurate for a CT data acquisition that will be used for the RT planning to record most of organ movements that occur during normal patient conditions. The result of this acquisition will provide with useful information about the movements of specific organs that might be located near or attached on a tumour, and vice versa. This information could assist the more precise assignment of the field size and orientation that will be used to treat the tumour.

Our main interest in this work reflects on the body surface movements of the patient. Principally the surface of the patient can be visualized in 3D using voxel or polygon based techniques. Usually the polygon-based techniques are used since the body contours can be defined and modified if necessary from the user. Then triangulation techniques are used to generate a mesh out of the final planar contours [Boiss88]. Based on the mesh surfaces several calculations must and can be performed during dose distribution calculation. In addition to communicate the body contour coordinates between different software systems in the radiotherapy department, the planar contour representation is used as standard geometric format. An important aspect during RTP is the calculation of the Source-to-Skin-Distance (SSD). This parameter serves several functions including the following:

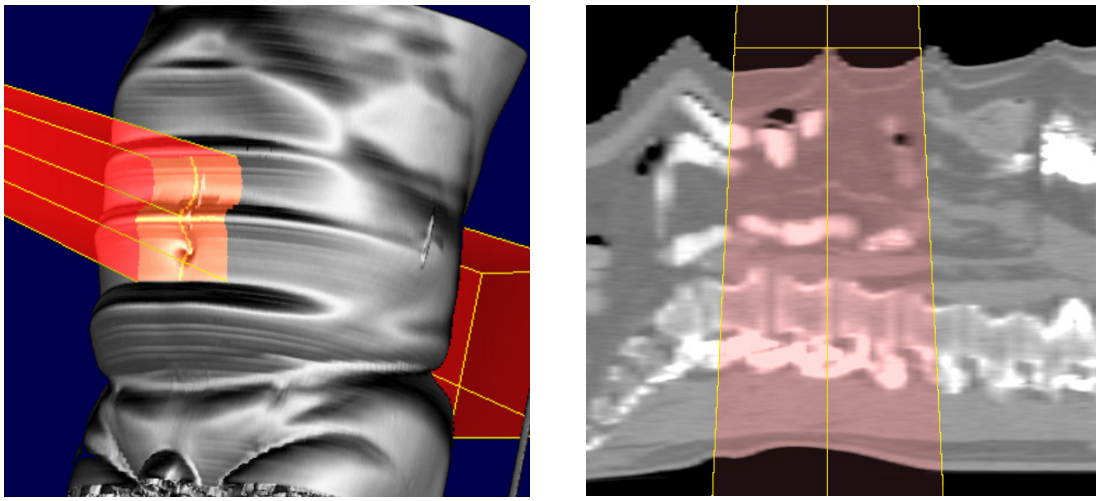

(a) (b)

Figure 4-1. Torso volume illustration with treatment field. In (a) volume rendering reconstruction of a male torso with an overlay of the 3D treatment beam. In (b) a 2D sagittal MPR of the CT data illustrating the iso-center placement of the beam on the crest of the breathing wave.

- Beam iso-center placement during geometric planning of the treatment and patient set-up verification prior to treatment.
- During dose calculation most commercial dose algorithms consider the body surface as the borders for starting the attenuation of the dose distribution on the target volume as well as on the organs at risk. Different anatomy of the body surface will result in variation of the dose distribution.

Hence it is common understanding in radiotherapy, that inaccuracies on patient's body planar contours will lead to inaccurate calculations and analysis related to the patient's body surface. In Figure 4-1 an example of surface reconstruction is presented where the treatment beam is projected over the patient's 3D surface. The corresponding sagittal view with the 2D beam overlay shows that considering the current volume information the iso-center of the treatment beam would be placed on the pick of the wave, which can be of course very misleading for the patient treatment.

4.2 Related Work

To our knowledge this is the only report trying to deal with the reduction of breathing artifacts on the patient's surface in RTP. Our method is motivated from previous reports appeared in computer graphics community related to polygonal meshes smoothing. Digitisation is a very common approach used to acquire the surface shape of complex geometric models. The 3D scanner technology enables us to capture detailed and dense clouds of points of objects surfaces. These samples are then organised into a triangular mesh for further development. However the original reconstructed models are usually contaminated with noise, and therefore mesh processing algorithms, such as mesh filtering, editing and mesh simplification are usually necessary for further refining of the reconstructed model. The Laplacian algorithm [Vollm99] is an approach that very often used for mesh fairing,

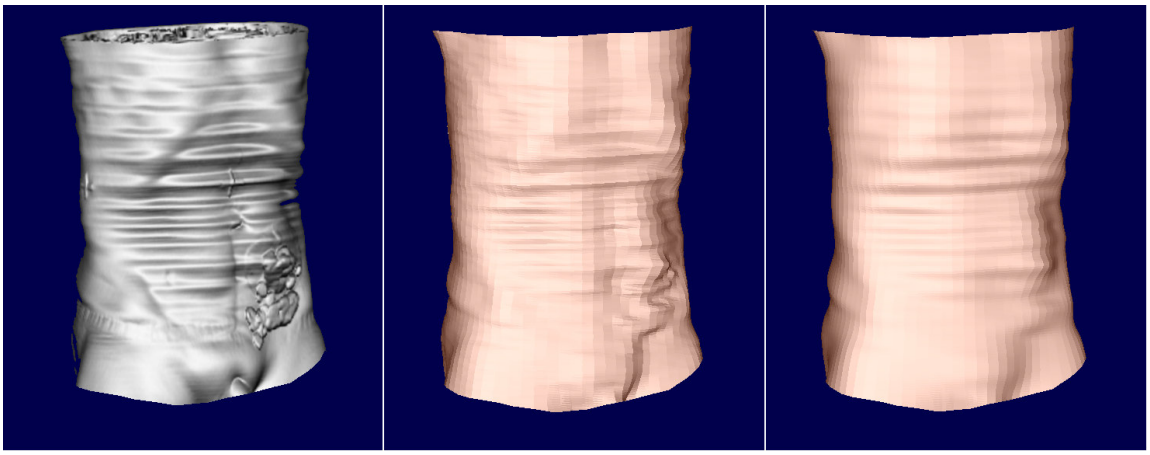

Figure 4-2. Most left-Original volume data reconstructed with volume rendering. Middle-The corresponding polygon model. Most right-Polygon surface after 60 iterations with the Taubin's explicit fairing algorithm

but results to serious shrinkage and distortion of the surface shape. This is the problem that most researchers addressed and tried to solve.

Taubin *et al* [Taubi95] first proposed the fairing algorithm for irregular meshes by adapting a signal processing approach. He adapted two derivatives of the discrete Laplacian, as well as an explicit iterative procedure to fair the meshes and minimise the shrinkage. Kobbelt *et al* [Kobbe98] used the *umbrella operator*, which basically stands for the discrete Laplacian. Their approach was combined with Taubin's to stabilise the result of the *umbrella operator* and was used in the construction of fair interpolator subdivision schemes. Vollmer *et al* [Vollm99], improve the Laplacian smoothing method to attenuate the shrinkage. The basic idea was to move the vertices of the smoothed mesh towards their previous location by some distance. Probably the most effective and stable solution to the faring problem is given by Desbrun *et al* [Desbr99]. In his approach, the implicit fairing was based on Laplacian operators that were used for the design of the low pass filter. For reducing the degree of mesh shrinkage a scale operator was used in combination with the Laplacian operators as well as constrain parameter of volume preservation. This parameter was calculated as the relation between the volume of the mesh at a smoothing iteration and the volume of the original mesh. In the same work the inadequacy of the umbrella operator in terms of mesh distortion is discussed, if applied on irregular sampled meshes. The proposed solution to the problem was a curvature flow process that was used to preserve sliding of the vertices of flat areas and curvature for constant curvature areas.

The techniques described above have as basis the umbrella operator that is calculated directly from the neighbour vertices of the centre vertex *p*. In every case the aim is to reduce the introduced noise at the reconstructed mesh or even for fine smoothing of the final surface. One requirement of the smoothing approach of course is the maintenance of the main characteristics of the surface, which represent the low frequencies of the mesh. Figure 4-2 illustrates a surface reconstruction of the abdominal region using volume rendering. The original volume data is composed of 165 slices that are equally spaced in 3mm distance. The breathing phases of the patient cause the abdominal region to expand and shrink. In the current example this process has been acquired as useful information

and can be observed on the skin surface as “waves”. The wave amplitude and phase varies from patient to patient but also in different time moments within the same study. The body contours from each slice have been automatically segmented and converted into planar contours. These planar contours have been used to reconstruct the polygon surface displayed in the middle image. As already mentioned in previous paragraph, these “waves” influence in several aspects calculations in radiation therapy treatment planning process. The goal now is to smooth the observed waves into an average position maintaining as much as possible the original mesh volume and basic surface curvatures. The most right image shows the results after applying 60 times iteratively the explicit fairing method as described in [Taubi95] without smoothing constrains. It is obvious from the results that this approach smoothens the small details, high frequencies, and maintains the main surface characteristics, low frequencies, quiet effectively without shrinking the original mesh. However the problem stated above is not reduced.

In this work a different approach compared to previous is introduced. Our method is able to minimize, and in some cases to eliminate, the motion artifacts introduced from to the respiration process in the CT data acquisition on the patient’s body surface. In the current method we consider as key step the extraction of the planar contours from the original CT data in a specific manner, following the motion of the breathing process as this is captured on the axial CT images. Important aspects at this point are the definition of the adequate number of sampling points that will compose the planar contour and will remain constant during the sampling process of every slice, as well as the location of the sampling points in terms of angular distance. The sampled points that compose the acquired contours will be filtered based on their angular value. This converts actually the mesh fairing problem into simply one dimensional signal processing. However the smoothing step will also cause deformation to the main features of the original mesh. Therefore we introduce constraints on the level of the planar contour as well as on the angular position. This allows the user to select specific level of axial contours from i to $i+n$, for smoothing. In a similar way angular ranges can be selected.

4.3 Generation of Body Surface

The breathing process is a complicate one and involves the combinatory work of several internal organs. Crawfort *et al* [Crawf96] generated a parametric model of the breathing process based on cross sectional images. Assuming that the acquired cross section image was with supine patient orientation, with the patient’s back resting on the scanner’s table, one can notice that breathing causes a time-varying magnification of factors *Mg(x)* and *Mg(y)* of the image in both image directions x, y respectively. Richies *et al* [Ritch96] in order to create simulated respiratory motion data, used a radial based warping function. The warping function consisted of angularity spatially and temporally varying magnification about a point at the posterior edge of the test object. Of course the above models are simplified ones since the physical breathing process involves also translation to the z direction, which is difficult to predict and correct based only on cross section images.

We also consider that the angular based magnification model represents better the respiratory process. In order to support this statement we consider an experiential comparison between different studies CT studies. Among 15-20 CT data sets of the abdominal and chest region most of them showed that the outer body contours translate similar to those illustrated in Figure 4-3. Both illustrated contours are extract from the original CT image on the same slice level and indicate the outer body contour in two different time

moments. Although the presented approach involves the correction of the motion artifacts between different slice levels the principle that will be used is similar. The magnification vector between the point $P(x,y)$ and $P'(x',y')$ could be easily calculated from the difference between the two points.

$$x' = x + dx \qquad \text{Eq 4. 1}$$
$$y' = y + dy$$

The parameter dx, dy is the translation vector that might have positive or negative values.

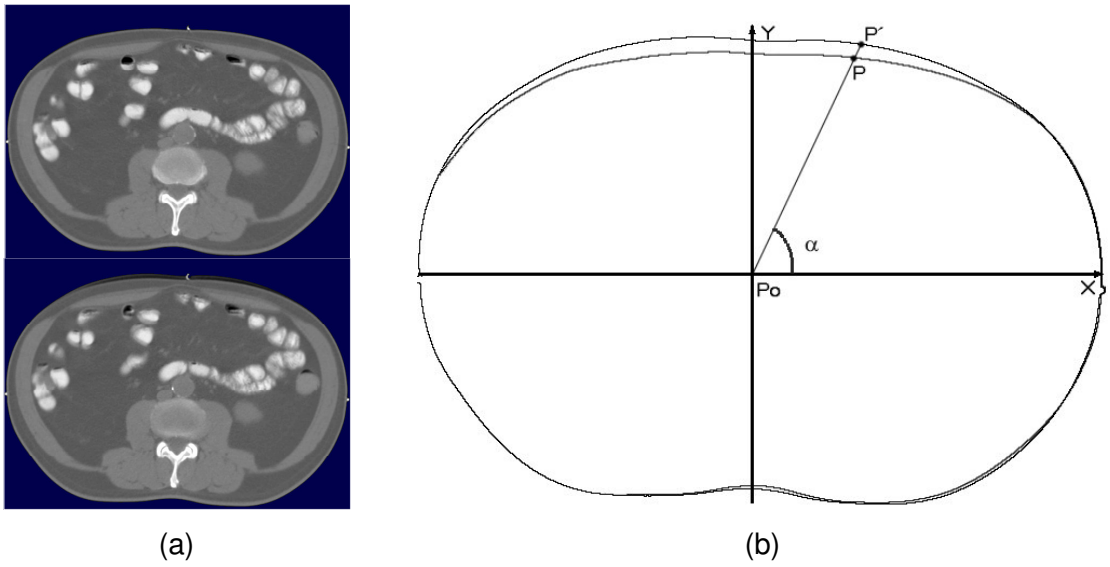

(a) (b)

Figure 4-3. Deformation of an axial body contour during breathing. In (a) two CT cross sections at two different time moments t and $t+1$. In (b) outline body contour comparison.

The point $Po(xo, yo, zi)$ represents the geometric centre of the volume bounding box. The breathing process is separated into inhale and exhale phase. The inhale phase lasts much less than the time of the exhale phase (see Figure 4-1). On can observe that the width of the picks is less than the width of the cavities. In that view the picks represent the frequency of the inhale process and the lower cavities the frequency rate of the exhale process. At this point we have to clarify that the collected digital images do not necessary describe the complete respiration process at every time moment. Some information might be neglected and some will appear as blurring artifacts due to low rate data acquisition. Aim of this work is to estimate and recover each contour deformation caused from the respiration process, in relation to the neighbour cross section images. By applying our method the magnification and shrinking vectors of the above model can be calculated automatically on each contour considering the neighbour contour deformation.

4.3.1 Generation of Body Planar Contours

At this point we need a few definitions. With ***X*** we will represent the polyhedral surface, $x_{i\alpha}$ a vertex of the surface at *i* slice level and α angle. In our polygonal surface we could have two types of neighbours of a vertex $x_{i\alpha}$. When the vertex is located at the same slice level and has different angular location then is indicated as $x_{i\alpha 1}$. When the vertex belongs to

the same angular location but in different slice level then is indicated as $x_{j\alpha}$. The edge connecting $x_{i\alpha}$ to $x_{j\alpha}$ is represented as $g_{ij\alpha}$. A discrete surface signal of the polygonal surface at a angular location α is a function of $S_\alpha=\{x_{i\alpha}\ ,\ i=1,2,3,\ldots,\ L\}$, where L the total number of cross sections.

The proposed methods can automatically extract from the original CT data volume the body planar contours. However the generation of the contours require two special conditions:

a) Every detected contour at each slice level must be composed from the same number of points. This parameter corresponds to the number of angular values *Ai*.

b) Every contour point at slice level *i* must be collected with the same angular value from the point *Po,* in relation to its neighbour points in slices levels $x_{h\alpha}$, $x_{j\alpha}$, where $\{h=i-1\}$ and, $\{j=i+1\}$.

The main reason for adapting this approach is the 2D inspiration model described in previous section. This model can by applied on the CT axial cross sections. The sampling points that will compose the final contour must be collected at specific angularity in relation to the central axis of the body bounding volume. This is necessary in order to be able for the filtering step to compose one-dimensional array from the sequence of points based on their angle value. These arrays will be the input data for the filtering function. The number of different angles that will be used for detecting the sampling points also defines the number of sampling points that will generate the planar contour. This sampling rate has no specific value but depends upon the user selection and the complexity of the surface that must be reconstructed.

The angular point-tracing algorithm (APTA) is based on a two-dimensional ray casting. The ray casting methods are well established in volume rendering techniques where the volume under investigation is sampled with multiple rays, which are emitted from the final image plane. To realize this concept a starting and an ending point of the ray must be defined. In volume rendering applications the ray points contain 3D information about their location. Depending on the camera model used during reconstruction the rays might follow parallel or perspective paths. In case of camera rotation the ray points are recalculated defining new directions for the ray paths. The most common approach used is a 3D digital differentiator analyser (DDA). The numbers of sampling steps that will be used for each sampling ray depend upon the resolution of the sampling rate and the accuracy of the final image.

To label the sampling voxel as the one belonging to the skin boundary region one could use a simple Hounsfield unit (HU) threshold value. However when sampling or processing images based on thresholds, the processing results become sensitive when dealing with noisy data as well as in case of not distinct organ boundaries. The most common problem appeared in our experiments were noise with high values appeared at the lower sides of the image, usually where the CT table is located. Therefore the precalculation of an opacity volume considered being necessary for optimising the collection of the sampling points. The opacity volume was calculated based on gradient operators, an approach established of [Levoy88] and used very often in volume rendering literature. The intersection point between the ray and the body boundary is selected based the opacity value of the voxel under sampling. Often the CT table-top where the patient is placed during scanning is included in the reconstructed slices. Currently it is extracted af-

ter manual definition of that level. In this work a specific approach is used for the generation of the body contours but the method is not restricted only to that principle.

4.3.2 Sampling Rate Selection.

For selecting the appropriate number of sampling points *Ai* that will adequately describe the body shape we select as criterion the comparison between the APTA contours and the original body contours as they are segmented using a boundary tracing method. At this point a quick but effective value is required in order to judge whether the calculated contour describes effectively the original body shape at the current cross section image. We consider the overlapping area as an adequate value for that comparison. The overlapping area is calculated for every contour belonging to a different slice levels. Then the mean value of the difference of the overlapping area is calculated. If this difference is above 10% then more angular points must be sampled in order to describe with higher detail the body shape. In our experiments we found that not more than 80 angle positions are required to describe the body shapes of the collected volume samples. For generating the triangulated mesh a very simple triangulation algorithm can be used by connecting the points that belong to different contour levels but on the same angular value. Examples of the conventional polygon reconstruction are given in Figure 4-2.

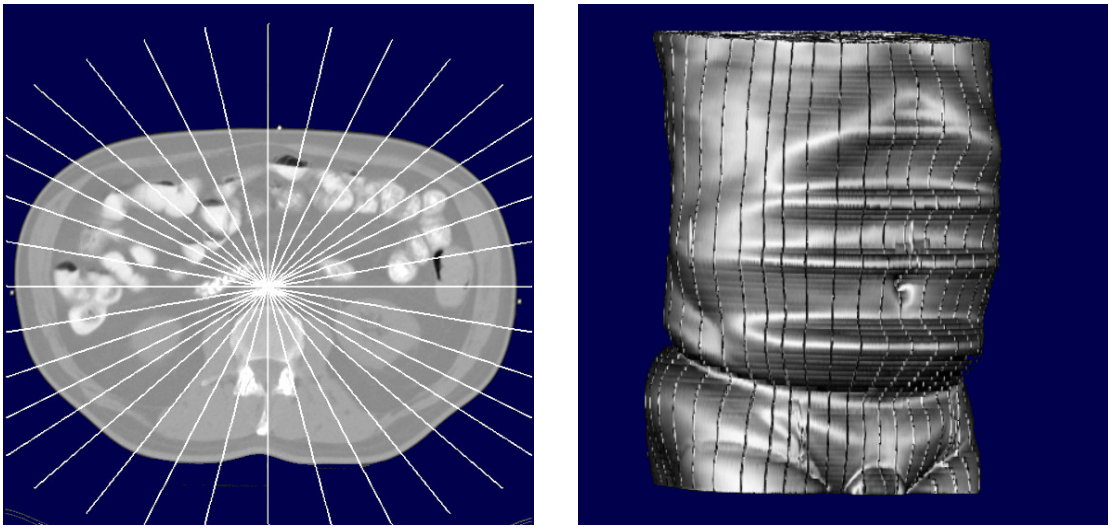

(a) (b)

Figure 4-4. Angular sampling rate selection. In (a) an example of radial sampling on a 2D cross section is shown. The 3D reconstruction of body volume (b) with longitudinal indication of the sampling rays (dark stripes).

4.4 Smoothing filter

As already mentioned the group of points that have been collected with the same angle, compose a group of one-dimensional signals that will be used as input in the surface smoothing algorithm. In the specific application we transact with very low frequencies and not with noise that represents high frequencies. The filtering process could take place in the frequency domain after decomposition of the signal to its frequency components. However this approach is computationally expensive and complex. Alternatively we con-

sider the low pass filters implemented by convolution. To distinguish between frequency and space domain we will refer with the term *low-pass filter* to the frequency domain and *smoothing filter* to the spatial domain. As primary smoothing filter for our application we consider the moving average since it can be implemented by convolution and aims to average the fluctuating values appeared in the signal.

The proposed surface smoothing approach aims to average the differences that exist on the longitudinal direction the breathing artifacts in order to minimize the skin (surface) distance calculations. The moving averaging (MA) filter is the first approach one could think to perform this task. The MA is the most common filter used in digital signal processing probably due to the simplicity in implementation and speed in performance. Although the MA filter is optimal on reducing random noise causes partial distortion on the original signal edges. The MA filter operates by averaging a number of points from the input signal to produce each point in the output signal. In equation form it can be written:

$$y[i] = \frac{1}{N} \sum_{j=-\frac{(N-1)}{2}}^{\frac{(N-1)}{2}} x[i+j] \qquad \text{Eq 4. 2}$$

Where $x[i]$ is the original signal, $y[i]$ the filtered signal and N the order of the neighbour samples or convolution kernel size.

In order to analyse the frequency response and performance let us consider a rectangular pulse of specific size as shown in Figure 4-5(a). The smoothing result of the MA can be amplified or reduced by controlling either the size N order of the neighbour samples or by maintaining a constant values N and performing multiple-passing of the MA. Figure (x)c illustrates the frequency response of the MA filter with different kernel size. On can observe that the MA filter has very poor frequency response. Small size of the kernel provides slow roll-off and poor stop-band attenuation. Even if the size of the kernel increases then it is still not possible to distinguish and isolate the high frequencies (see Figure 4-5(a) & (b)). By applying the filter with multiple passes we obtain an improved frequency response in comparison to the increased the kernel size. After 2 passes with the original MA kernel, the input rectangular pulse response has been converted into a triangular filter kernel. By continuing this process the shape of the kernel converts to a bell shape quiet similar to the Gaussian smoothing kernel, with attenuated amplitude. Actually this is the behaviour we request from a smoothing filter for our application since we have to suppress very low frequencies. The frequency response of the multiple pass MA filter is illustrated in Figure 4-5(c) & (d). The frequency response of the 4-pass MA filter can isolate the and completely cut off high frequencies. As one could expect the frequency response of the 4-pass MA is very similar to the frequency response of the Guassian smooth kernel. As Oliensis *et al.* [Olien93] pointed out et al the Gaussian kernel produces shrinkage because it is not a low-pass filter. Basically except the zero frequency all the frequencies are attenuated.

Filtering examples of the MA filter with multiple passes are illustrated in Figure 4-6. Two curves with different frequencies have been selected. A signal describing low breathing frequency is shown in Figure 4-6(e). High respiration frequency is shown in Figure 4-6(f). The last curve actually corresponds to the normal breathing conditions. The MA filter was applied to both curves iteratively for seven times. The dotted curves represent the

averaged result of the original curves. The higher picks of both curves have been flattened elevating at the same time their lower region.

$$\mu(i) = \frac{\sum_{i=1}^{N} x(i)}{N} \qquad \text{Eq 4. 3}$$

$$SD(i) = \sqrt{\frac{\sum_{i=1}^{N} \left(x(i) - \mu(i)\right)}{N}} \qquad \text{Eq 4. 4}$$

$$SDE(i) = \frac{SD(i)}{\sqrt{N}} \qquad \text{Eq 4. 5}$$

4.5 Surface Smoothing

4.5.1 Surface Signal Constrains

The proposed approach is applied to the complete data volume. The developing of an algorithm that automatically could detect the regions that include breathing artifacts is a difficult issue. The main limitation for such an approach is the body curves, which might have very similar frequency to the noisy curves. Therefore the algorithm should be applied on specific regions of the collected CT data. Basically there is two types of constrain that must be defined: the angular and the longitudinal constrains. The angular refer to the numbers contour points, which represent angles between the body surface and the body central axis of the body volume and the external surface position. These constrains could be applied as constant values since the breathing deformation effects specific regions of the patient's sides.

The second type of constrains, the longitudinal, are the most significant for producing accurate results and must be placed manually. The user can select the appropriate slice level in both directions cranial and caudal. In order to maintain continuity at the region of constrains among the original and filtered data the smoothing process is applied to the complete patient volume and the filtered results are merged with the original data at the constrain boundaries using linear interpolation. This concept is illustrated in Figure 4-6. The marks on both images illustrate constrains in the longitudinal direction. The smoothed curve Figure 4-6(a) has a rapid reduction value at the constrain points. This is eliminated after applying the linear interpolation between original and filtered values as shown in Figure 4-6(b).

4.5.2 Control of Filter Iterations

Most mesh fairing schemes require the manual adjustment of the filter iterations. In other words the user will decide for the level of smoothing that will be applied on the specific mesh. In some case this level can be predicted, e.g. when dealing only with noisy data. The semi-automatic control of the filter iteration process is a great mechanism

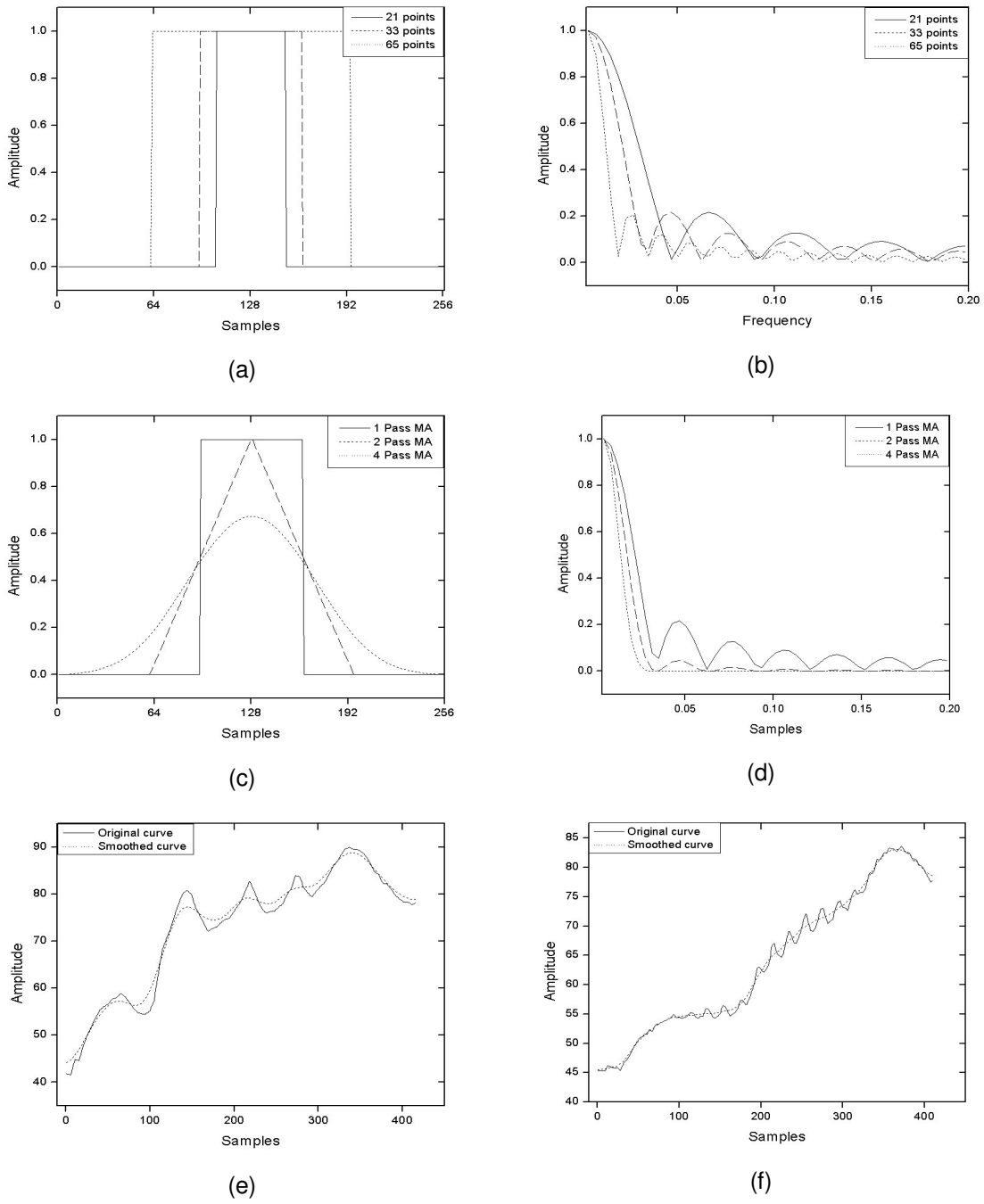

Figure 4-5. The moving average filter and filtering examples. In (a) and (b) MA kernel examples and their frequency response, using different kernel sizes. In (c) and (d) MA kernel examples and their frequency response using iterative filtering. In (e) and (d) filtering results on different respiration frequencies.

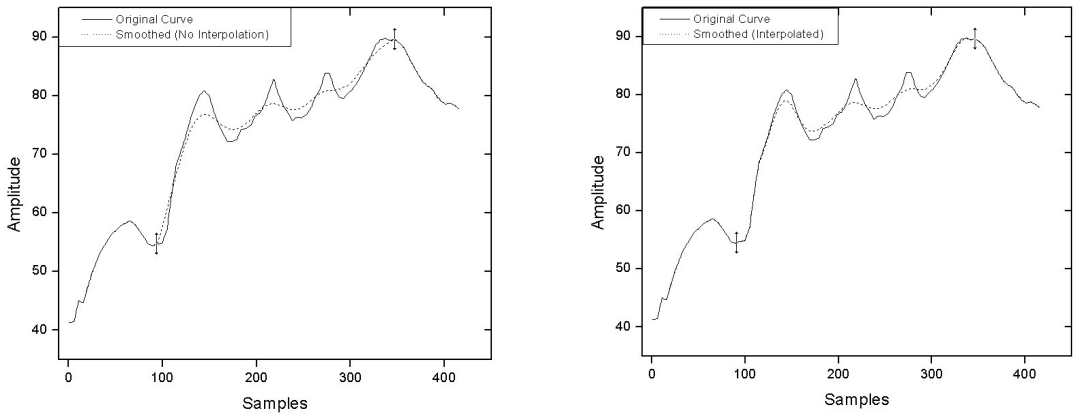

(a) (b)

Figure 4-6. Comparison between interpolated and non-interpolated smoothed curves. In (a) the filtered curve using the MA filter and after applying two constrains. In (b) the same filtering results but after applying linear interpolation at the constrain levels.

for a mesh-fairing scheme since minimum intervention is required from the user.

In order to automatically control the number of iterations of the smoothing filter the SDE is used as comparison criterion. After the first iteration the summation of the percentage of the error difference between the original and the smoothed surface is calculated. The calculation takes place on each angular curve that is involved in the smoothing process. The individual SDE are added to generate the final value. The equation form of the above description is as follows:

$$\Delta_{SDE}(i)\% = 100 \cdot \frac{SDE_o(i) - SDE_f(i)}{SDE_o(i)} \qquad \text{Eq 4. 6}$$

$$T_{SDE} = \sum_{i=\omega 1}^{\omega 2} \Delta_{SDE}(i) \qquad \text{Eq 4. 7}$$

Where SDE_o, SDE_f, are the standard errors of the mean for the original and smoothed curve respectively at the angular value *i*. The value $SD_o(i)$ is the standard deviation of the original curve at angular value *i*. *N* is the total number of samples in the longitudinal direction (also corresponds to the number of slices). The value Δ_{SED} stands for the percentage of the difference between original and smoothed SDE values and T_{SED} for the total summation of the Δ_{SED} values.

The first value of the Δ_{SED} can be considered as an indicator of the quantity of the filtering effect on the original surface. If Δ_{SED} has large value then the difference between the original and filtered surface is high and vice versa. The iteration loop will stop when the value of the T_{SED} reached four or five times the value of the first calculated Δ_{SED}. This approach work very efficiently as automatic prediction of the number of iterations for low and high frequency breathing artifacts.

4.6 Results

The purpose of the performed measurements was to assess the contribution of the proposed surface smoothing method on the correction of the shape of the original body contours. The proposed method was evaluated using 15 CT datasets from arbitrary selected subjects that were scanned in the abdominal and pelvic region. All subjects were scanned at free inspiration conditions using spiral CT (Siemens Somatom Plus 4). The average number of slices collected from each scan was 85 per patient, 3 or 5mm thin with equal slice distance respectively. For every volumetric data the original body contour was extracted using the *APTA* described in section. Surface signal constrains have been applied manually on different slice levels every subject surface. These constrain aim on protecting the main features and curvatures of the original body surface from deformation after surface smoothing.

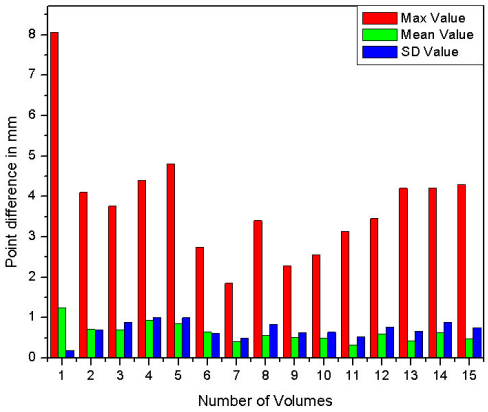

(a)

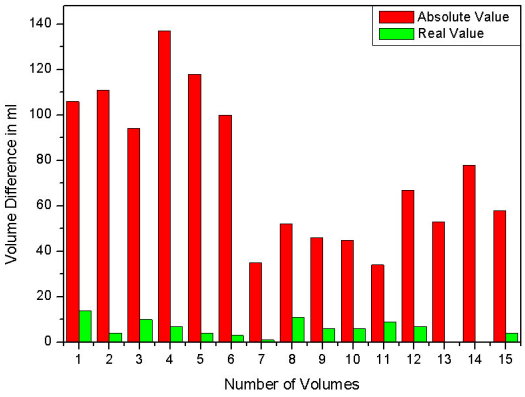

(b)

Figure 4-7. Results of quantitative comparison between original and reformatted torso-contours. Results in (a) show differences single contour points. Results in (b) show differences between original and smoothed volumes.

For each contour point we estimate the Euclidean distance between the original and the reformatted contours. The border positioning accuracy, was assessed by computing the *Mean* value, the *SD* value and the *Maximum distance* (*Max*). This method gave us the maximum difference between vertices of the original and the smoothed surface. The second criterion used was the total volume of the original and the filtered surface objects. A very common method for estimating the volume of closed mesh surface is described by Lien. However for open surfaces generated from contours one can calculate the surface of each contour, multiplying the final result with the corresponding slice thickness. The total interior surface volume will be given after adding the volume of each slice. The preserved interior surface volume of the smoothed surface can indicate that the filtering process did not cause severe shrinkage to the polygonal surface. This concept is very important is a very important property required in our application. However the interior surface volume does not provide any information level of smoothing on the original surface. For assessing the absolute variation of volume between original and reformatted mesh the partial volume variations was used. This parameter was calculated on each slice level as the absolute difference between original and smoothed contour volume. The total value of the absolute volume differences between original and smoothed mesh, was

estimated after addition of the partial volumes. These measurements provide a good factor for understanding the effect of the smoothing process.

The numerical results of the smoothing process are presented in Figure 4-7. The top chart presents the maximum the mean and the SD of the distances between original and reformatted contours of the complete contour set, for every volume sample. Among 15 volumetric CT data, which result to 1450 body contours, the maximum contour difference was 8mm and the minimum 2mm. The maximum mean value was 1.2mm with SD ± 0.2mm. The reason for the low mean values is the small amount of contour points that where repositioned at each contour. The absolute and the actual differences between

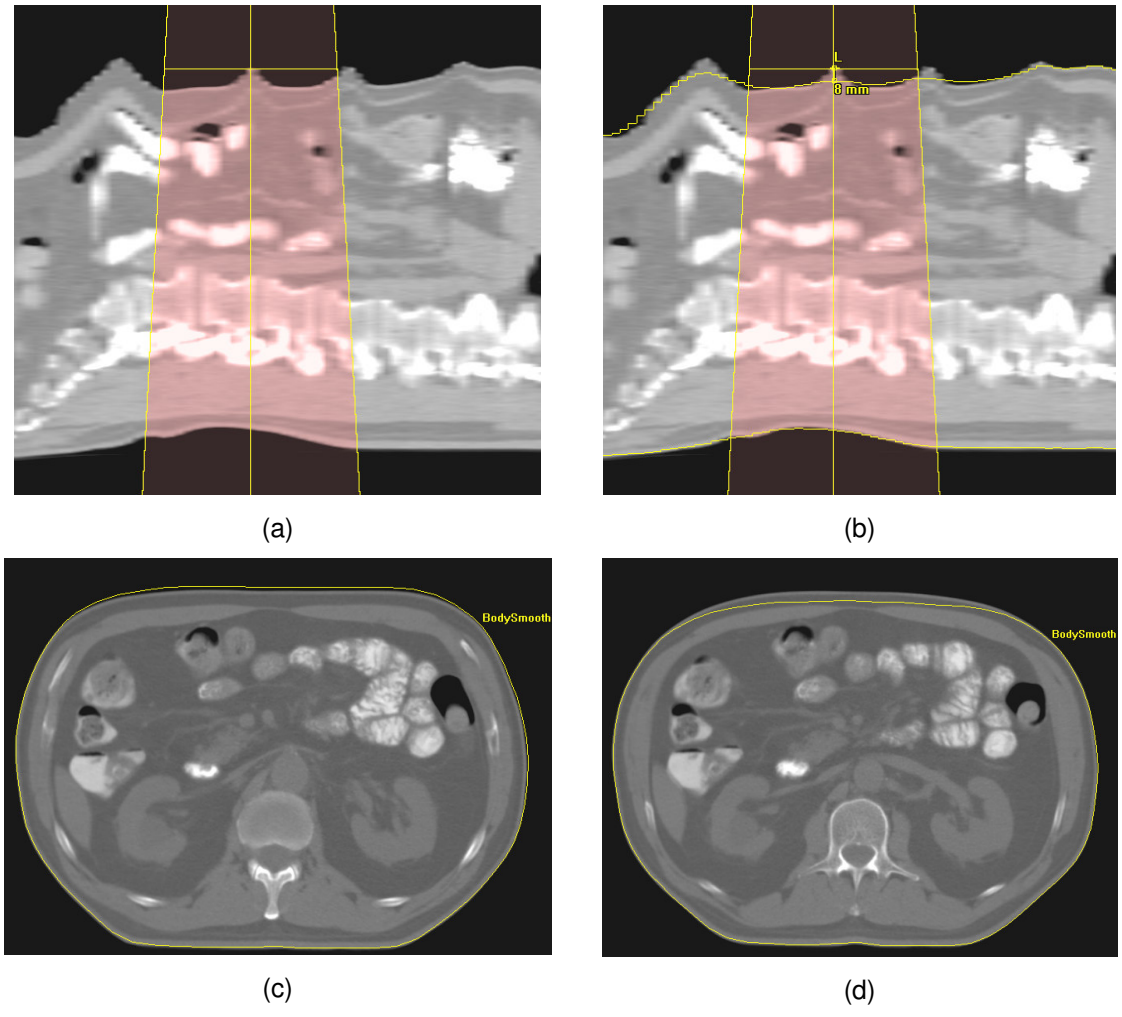

(a) (b)

(c) (d)

Figure 4-8. Comparison of contour smoothing results. Sagittal images (a) and (b) show the difference between original and proposed position of the beam iso-center. In (c) and (d) two different slices are used to indicate the difference between the original axial slice and the proposed contour.

original and smoothed surfaces are illustrated in the lower graph of Figure 4-7(b). The mean value of the original sample volumes was 22101ml. The mean value of the actual volume difference was 8ml, a very small value compared to the average volume of the all sample data. This certifies that the proposed method caused no shrinkage to the mesh volume. The maximum value of the absolute difference in mesh volume was 137ml and

the mean value 75.6ml with SD ±33.08ml. This volume variation represents only the 1% of the original mesh volume. However if one considers these variations locally then the influence in measurements can be valuable. Figure 4-8 illustrates the smoothing result of our method on a 2D image level. The sagittal images in Figure 4-8(a) and Figure 4-8(b) show the differences between original and proposed position of the beam iso-center. In the specific example up to 8mm contour distance has been corrected using our method. In Figure 4-8(c) and Figure 4-8(d) two different slices are used to indicate the correction effect between the original axial slice and the proposed smoothed contours.

The 3D surface smoothing results of the approach are shown in Figure 4-8. For visual

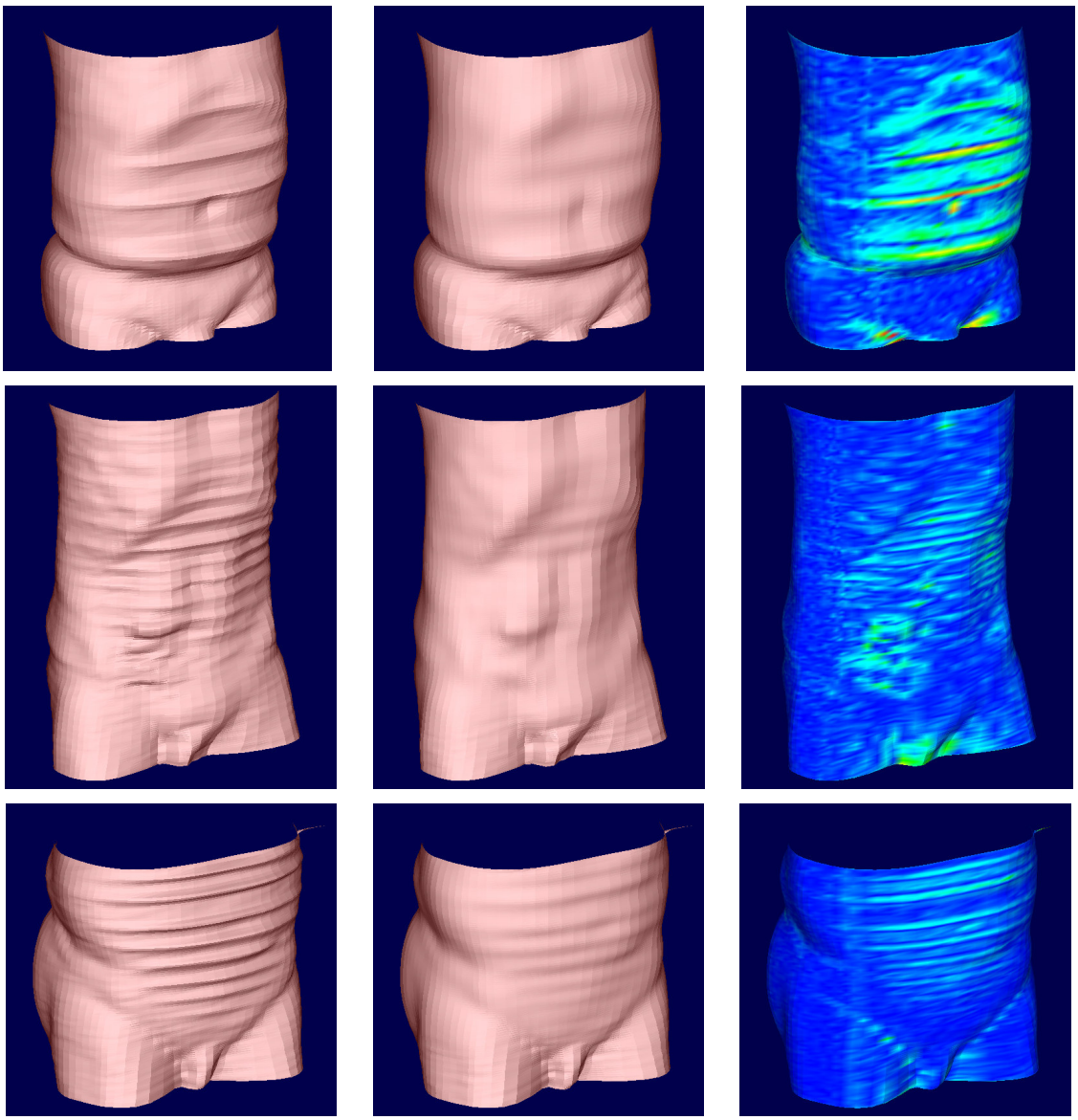

Figure 4-9. Different surfaces smoothing examples. Notice that the respiration artifacts are not developed uniformly but vary between high and low rates. The left column represents the original meshes. The middle the smoothed-reformatted. The right colour-mapped mesh indicates the areas with modified vertices.

comparison of the smoothing effect a colour-map index is given over the smoothed meshes. An optimal factor for the SDE was used to control the number of iterations of the smoothing process. This factor was the same for all sample data. However the number of iterations varied from 6 to 18, upon the frequency of the deformed surface. The estimated average number of iterations was 7. The processing time required for the smoothing of the surfaces depends on the number of vertices that compose the mesh. On the experiments performed in this work the mean value of vertices were 12200. In any sample case the processing time required for smoothing was below 1second on a Pentium III 933 MHz.

4.7 Summary

In this chapter we point out the affects of the respiration artifacts on torso surfaces reconstructed from CT data. The use of inaccurate information might lead to wrong calculations during RT planning and simulation. Considering previous models for correcting motion artifacts in CT imaging we can analyse the respiration process and correct it. Hence, a dedicated automatic approach is presented for the compensation of the respiratory artifacts on medical body surfaces reconstructed from planar contours. The method can handle fast and efficiently several types of body surfaces with respiratory artifacts that might include constant or arbitrary respiration frequencies. The system can detect and generate the body contours and surface automatically, and eliminate the respiration artifacts from the problematic regions. The user can define manually constrains on the angular or on the slice level. So far we cannot estimate how the proposed method will influence the results on the clinical environment. This is one part of our future work. In addition we investigate the development of a deformation model that will also compensate the movements of internal structures that deform during respiration.

Chapter 5

Improved Volume Rendering of Thoracic CT-Volumes

5.1 Introduction

Three-dimensional visualization in treatment planning is used to express information regarding radiation beam registration with the tumour, extend of disease and conformity of dose distribution to the target volume and organs at risk [Chen96]. Failure of radiation therapy to control the local or regional component of the malignancy can be due to misleading visual information in one of the above steps. The difficulty of delineating target volumes has been extensively discussed in the literature. However the increasing emphasis on 3D conformal therapy, with the more complex fields, increases the importance of accurate anatomic delineation and 3D representation. As mentioned in previous chapters, CT has been key to the development of the 3D treatment planning, providing the necessary anatomic information. Nowadays spiral CT provides high-resolution data, increasing the number of slices in a study, preventing the generation of motions artifacts and enhancing the boundaries of anatomical structures. As topographic information increases, various methods of display may be used to re-express this data into meaningful images, as demonstrated in Chapter 2.

In Chapter 3, volume segmentation methods have been briefly discussed, in order to extract volumes of interest from a series of tomographic images. In RTP these volume are necessary for display as well as quantitative purposes, such as dosimetry and volumetry. The communication of the geometric information of these structures among different planning software can be done only means of 3D coordinates of the object primitives. Traditional 3D visualization in radiotherapy planning, mostly in treatment planning systems, has been wire-loop and polygon based, typically requiring manual segmentation on consecutive CT or MR slices [Peliz98]. Despite the availability of several automatic segmentation tools, a significant portion of this task is manually performed, and can be time intensive for the user. In addition manual segmentation is binary process since the user must identify areas that sharply represent structure boundaries. The result of this process can be a polygon or voxel representation of the structure of interest. While these models provide useful information regarding the general anatomic and geometric relationships of the structures, permitting interactive BEV and OEV display, fine details of anatomy are typically lost. Polygonal models and binary voxel models, fail to represent the smooth transition of structure surfaces occurring at interfaces between tissues, and often do not preserve the sense of 3D connectivity. For this reason polygon render images they have not proven entirely satisfactory for displaying complex anatomy.

5.2 Related Work

In many radiation treatment planning instances, a geometric model of a given anatomical structure is not necessary. Common examples are patients that will receive palliative

treatment where no target volume is required. Patients with Hodgkin's disease are mostly treated with two mantel fields, typically from anterior to posterior direction (AP) and posterior to anterior (PA) isocentric beams. The field size and block beam apertures are designed directly on the DRR lack of and target volume and organ at risk. Similarly for patients with breast cancer, during whole breast treatment irradiation, the radiation field arrangement is performed based on the BEV. For the physician it is usually sufficient simply to appreciate the relationship of a target volume to surrounding normal organs. This might involve the visualization of the occlusion of several structures when viewed from a particular perspective. When the volume viewed from the BEV, perspective view, then the user can assess the potentially irradiated structures enclosed in the irradiation field superimposed. The alternative is to use the OEV, orthogonal reconstruction, where the radiation fields reconstructed as opaque or semitransparent polygons are projected with the original CT volume. An additional verification tool can be the use of the virtual light field that presents the intersection of the beam volume with treatment volume.

Pharynx, lungs and trachea belong to the category of the most important organs in the neck and thoracic region. Lung tissue is the one of the dose-limiting structures and it can be exposed in during irradiation of breast tumour, malignant lymphoma and intrathoracic tumours. On the other hand trachea is very often used as organ for orientating the physician during treatment planning of chest and neck tumours. Thus there is a vital importance on visualizing these structures in 3D in relation to neighbour anatomical volumes of the neck and chest region [Kuszy95], [Butke96]. There are several research works, which are capable to segment the lungs and the trachea volume semi-automatically. The most of them are voxel-based and use morphological approaches like region growing [Brown97], [Dehm99], [Hu01], [Shiyi01]. On the other hand an important issue is the visualization of those structures. Seemann et al. [Seema01] presented a hybrid approach for the 3D visualization of the chest for virtual endoscopy. In this work the airway volume have been segmented using the region growing approach. Then the corresponding volume was re-expressed as a triangulated surface. Usually the user must define an initial point and then the volume of the structures are filled, assigning a validity flag to those voxels that are identified as belonging to the structure under segmentation. Even if the segmentation algorithm provides fast and accurate results, a refinement of the final segmentation result is required due to several problems that might occur during segmentation. The use of the above methods can be optimal if the geometric information of the structures are required.

Pelizzari *et. al*. [Peliz96] described a volume rendering principles applied on the treatment planning using CT data. Principally he presented visualization options for the 3D reconstruction of soft tissues of the male pelvis. The use of a translucent "tunnel" when screening the volume from specific viewing directions, allowed reconstructing the structures of interest with high intensity and the rest of the volume with reduced intensity. Thus the irradiation volume could be interactively emphasised. In a more recent work Lee *et. al*., [Lee99] visualized with volume rendering the region lower head and neck. They used an opacity volume extracted from CT data, which have been acquired after injection of contrast medium, where the user could define the opacity of various tissues, prior to rendering. The result of this work demonstrated that organs like the lymph nodes the, salivary glands, vessels, and airway are visualized in detail without prior manual segmentation. Despite their positive general conclusion, their method could not eliminate partial volume effects (PVE) on the neck region that could obstruct the viewer from useful information.

In this chapter, we will partly explore the application of volume rendering in 3D virtual simulation of external beam and propose new volumetric visualization schemes for the anatomical regions of neck and thorax. Our focus will be the interactive visualization of

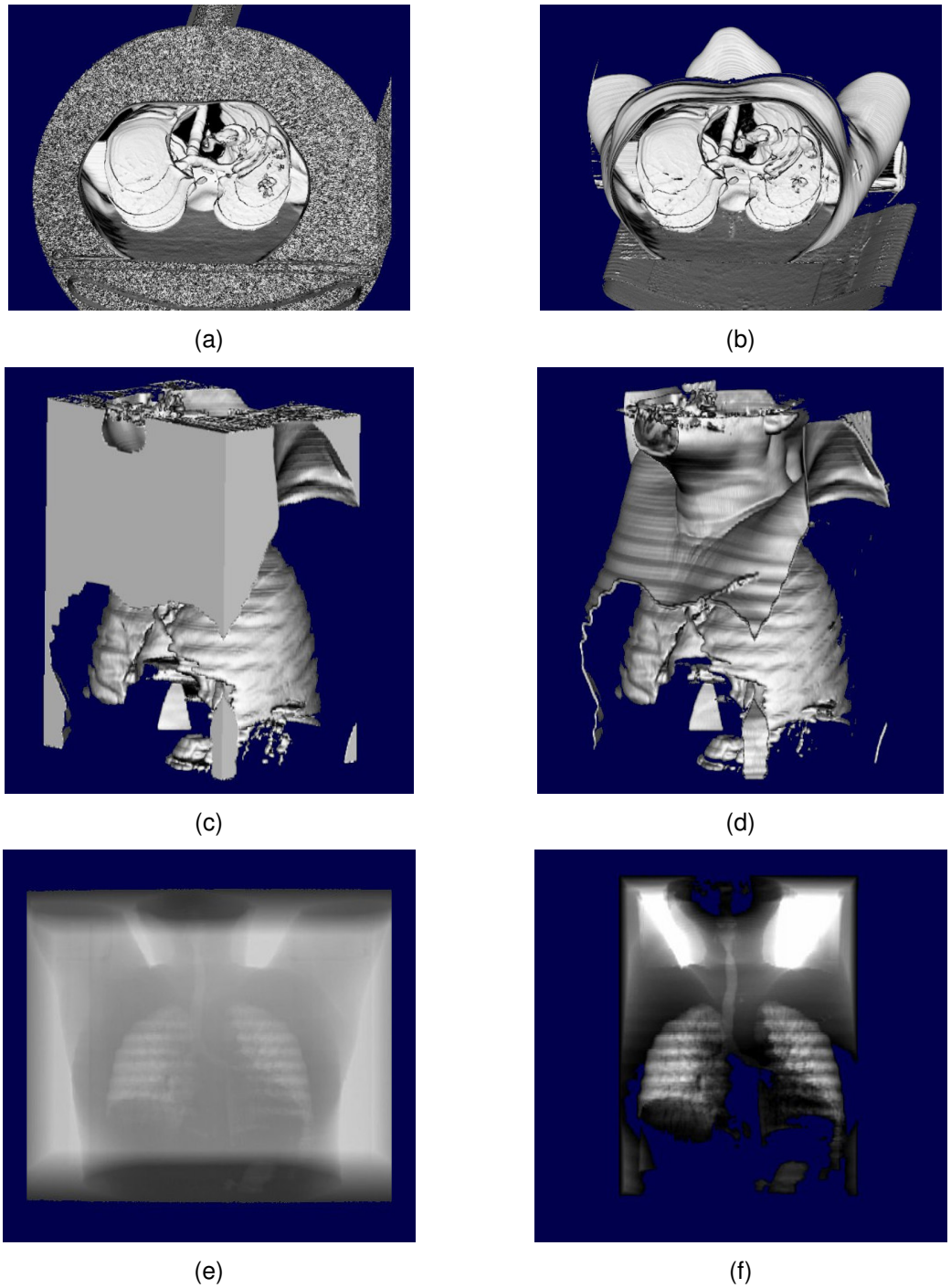

Figure 5-1. Reconstruction of the CT volume using direct volume rendering. Surface reconstruction is produced using iso-value (a), gradient opacity (b) volumes. In (c) and (d) the same information after applying a volume clipping box. DRR images are shown in (e) and (f).

the soft tissue of the chest region, in CT data that are acquired with conventional methods without prior manual segmentation. We believe that we give a very simple but effective solution to the PVE that occur on the skin surface, which is one of the problems the authors had to deal with in previous research work. The clear visualization of the trachea and lung volume from arbitrary viewing directions is not possible due to the skin surface of the neck and chest, which partially obstructs the view of these structures. The main idea is to use a region-growing algorithm at the data pre-processing step, in order to extract the background volume and skin surface and store it in a binary volume. Our aim is not to eliminate the semi-automatic or automatic segmentation procedures. In contrast we propose a visualization concept that will be of clinical use for several treatment cases, when volume segmentation is not required improving the rendering contrast of the soft tissue structures. For practical use these algorithms should perform the above operations in real time with minimum user interaction.

The volume shading methods used to display the results, involve those who are opacity based, metallic surface shading and transparent model reconstruction, mainly means of DRR on the BEV, with manipulated tissue absorption of the X-ray model. In addition the volume rendering algorithm used in this work is a hybrid ray casting capable of handling both polygon and volume data. In this instance the use of the Z-buffer principle allows us to reconstruct the radiation beam geometry in 3D as semi-transparent polygon object together with the volume data, as well as the projection of the virtual light field on the surface of the visualized structures at that level where both volumes, radiation beam and structures, intersect. The proposed approach gives a very clear illustration of structure surface and the their geometric interaction with the radiation field(s) in real time.

5.3 Conventional Volume Rendering

In Chapter 2 we first introduced the importance of volume rendering in RTP and virtual simulation. Volume rendering techniques is a family of methods for visualizing sampled scalar or vector fields of three spatial dimensions without fitting geometric primitives to the data. Volume rendering was introduced from several researchers in the context of medical imaging. The main volume visualization algorithm used in this application has been described in Chapter 2. Briefly our method involves ray casting through the data, and performing shading calculation along rays. The definition of the opacity map function attributes like colour and transparency are assign to the tissues types. This allows the user to selectively enhance or suppress structures of various intensities. As result such reconstruction methods can eliminate the explicit manual contouring step of structures in cases that is allowed.

If one attempts to reconstruct the lung and trachea volume using the standard gradient and iso-value opacity calculation functions as described from Levoy [Levoy88], then the result will be very similar to the one illustrated in Figure 5-1. Image Figure 5-1(a) illustrates the volume rendered from the iso-value opacity volume. The image is covered from noisy values, which represent the room air, and are the dominant voxels of the opacity volume containing very small HU. On Figure 5-1(b) the same CT volume is reconstructed from the opacity volume, which has been calculated using the gradient model. The result in this case is much better since background voxels can be omitted and the skin surface is clearly visible. However in both image illustration of the lungs and the trachea is possible only and from specific viewing directions. A partial solution to the above problem could provide an orthogonal volume clipping function that could remove part of the original vol-

ume in the three main directions Figure 5-1(c) and (d). In this case the clipping planes are adjusted manually and they move parallel to the main axis of the volume data. In radiotherapy this is a quiet useful functionality since the table support of the CT can be removed in order to observer the treatment field interaction with the posterior of the patient. Thus more interesting results can be produced when reconstructing the volume form a posterior point of view. Since the CT acquisition has been made using a flat tabletop the back of the patient has parallel alignment to the coronal volume-clipping plane. Limited information can be obtained also when using transparent illumination such as DRR. In this case the transfer function used has been modified such as the lungs and trachea are reconstructed as opaque organs having high absorption coefficients and the rest of the tissues as non-opaque objects. However in the reconstructed results the room air volume obstructs the clear view of the trachea and the lungs.

The use of the clipping planes is a significant improvement to the visualization results, but still not the optimum. Let us try to identify the reasons that lead to the above result. Figure 5-2 illustrates a single axial CT slice at the level of the thoracic region. The top left image is the original CT slice. The rest of the images illustrate the result after applying different contrast enhancement methods on the original image. The top right is the result of a triangular LUT for adjusting the image contrast. The lungs and the boundary of the trachea wall are clearly visible. Similarly the lower right image produces clear results of the wanted structures, improving the visualization of boundary structures. In both image result mentioned above, except the wanted structures, the skin boundaries are also visible. The

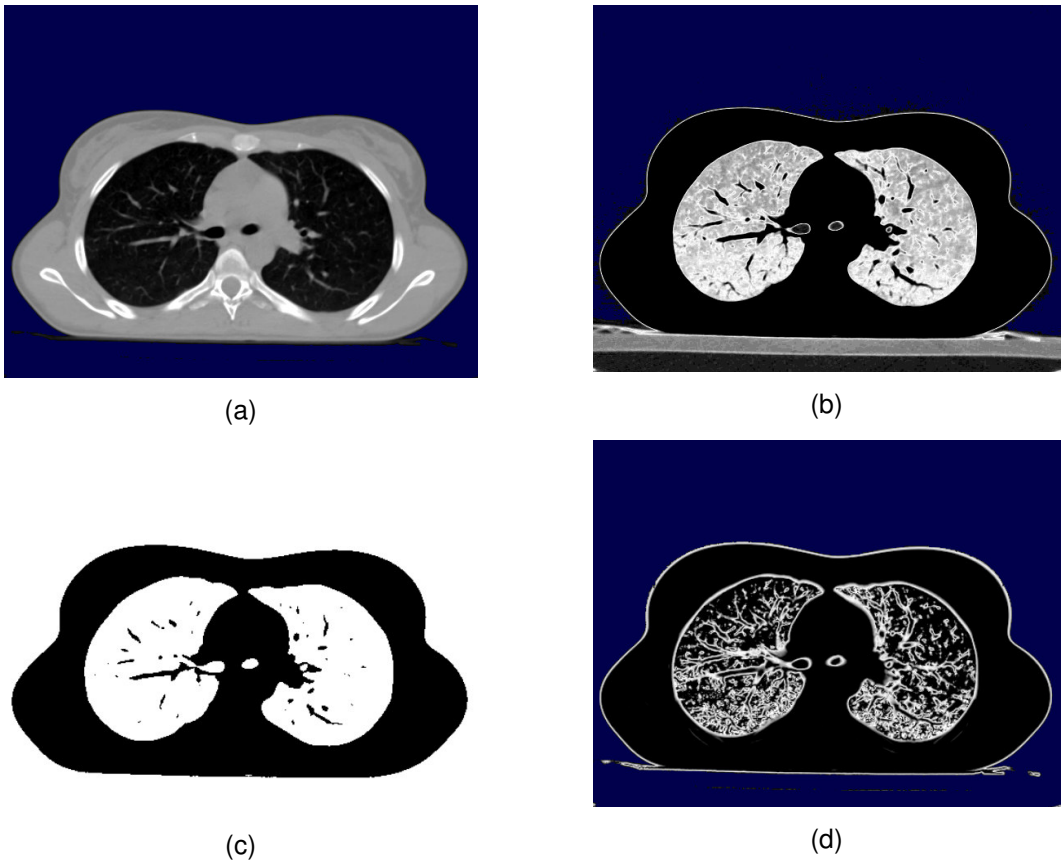

Figure 5-2. Examples of CT image windowing and edge enhancement.

lower left image illustrates the result using the iso-value (rectangular) LUT. In this case the wanted structures are illustrated as opaque objects but as well as the image background. These image examples illustrate very clearly that the HU values of lung and trachea borders are similar to the skin borders.

This problem is due to the partial volume effect (PVE), which is a well-known in medical imaging. When the object under scanning varies rapidly over distances comparable to the spatial resolution, one expects the voxel value to reflect the average value over the resolution element. In X-ray CT, a non-linear effect and artefacts can result when the object structure or edge detail occupies only part of the X-ray beam measured by a single detector element. Before reconstruction, the X-ray intensity measurements are converted into attenuation measurements by taking the logarithm. If a structure only intercepts part of an X-ray beam path, the measured intensity will be the average of the intensity over the X-ray path, and the resulting attenuation measurement is not the same as the average attenuation over the X-ray path. This effect is demonstrated in Figure 5-3, where a line sample represents the corresponding HU values of the CT image. One can clearly observe the HU variations at the boundary level of the skin, lungs and trachea. This 2D example demonstrates that it is very difficult to isolate on 2D or 3D level the lungs and the airway using thresholding techniques based on LUT.

So far there have been several methods proposed for the compression of the PVE artifacts that obstruct internal organs when 3D reconstruction methods are applied. A tissue classification method has been employed in combination with a multi-dimensional opacity function [Sato00]. The response of those filters and the original intensity values are used to define a multidimensional feature space in which multi-channel tissue classification strategies are designed. The applied method improved the overall quality of the 3D rendition. Beier *et al.* [Beier98] reported a method based on morphological filters in order to reduce the PVE for the reconstruction of diagnostic lung and brain volumes. The applied method, which was a combination of 3D dilation and erosion procedures, was capable to reduce the PVE on the surface of the above structures. Statistical models of PVE that assumed a Gaussian system for noise and fundamental material variances with Gaussian statistics have been proposed from Santago and Gage [SanGa95]. One of the most recent reports by Siadat [Siada01] combination of the intensity and structure information is used in identifying and overcome PVE. Their method utilizes a fundamental concept known as scale. The *scale* indicates the local structure size, which is determined at every voxel in a given image based only on intensity homogeneity criterion. The basic premise is that regions of small scale represent regions of potential PVE. Their method has been user to remove superficial (skin layer) artifacts in CT data.

In our concept we have to extract the background image volume and not only eliminate the PVE from the skin. Therefore we employ the following idea: Imagine that the background region of the CT volume (room air), is extracted together with the thin layer of the skin surface generated from the PVE that obstructs the viewing of the internal structures. This could be a binary volume with value one (1) when the region of interest is selected, room air and skin surface, and zero (0) for any other structure. For detecting this auxiliary volume we propose the use of a 3D region-growing algorithm. In order to reach the optimum result we propose the following processing steps:

a. Loading of CT data and store it into the main memory. Calculate the gradient volume using predefined parameters.

b. Select a default location for the seed voxel in order to initiate the region growing (RG) algorithm. In this step the background-auxiliary volume (BV) will be filled.

c. Apply opacity volume calculation using the BV exclusively.

The following paragraphs explain with detail the function of the above steps and the way to realize-integrate them in main visualization pipeline. Examples of single surface reconstruction using the opacity volume are given including DRR examples of the isolated volumes of the lungs and trachea. Further the optimised results of the full tissue range DRR combined with the surface reconstruction mode are presented demonstrating the advantages of the implemented method.

5.4 Region Growing

The region-growing (RG) algorithm is used very often in the region-based segmentation techniques and has been successfully incorporated into several medical imaging applications for the extraction of organ volumes [Masut96]. In this work we follow a simple design principle since the region boundaries that must be detected have low complexity and high contrast differences with the surrounding tissues. The RG algorithm is initiated with a seed voxel selected manually, which is known to be a part of the voxel of interest, room air or skin surface. If the difference in grey-level is between the voxel under investigation

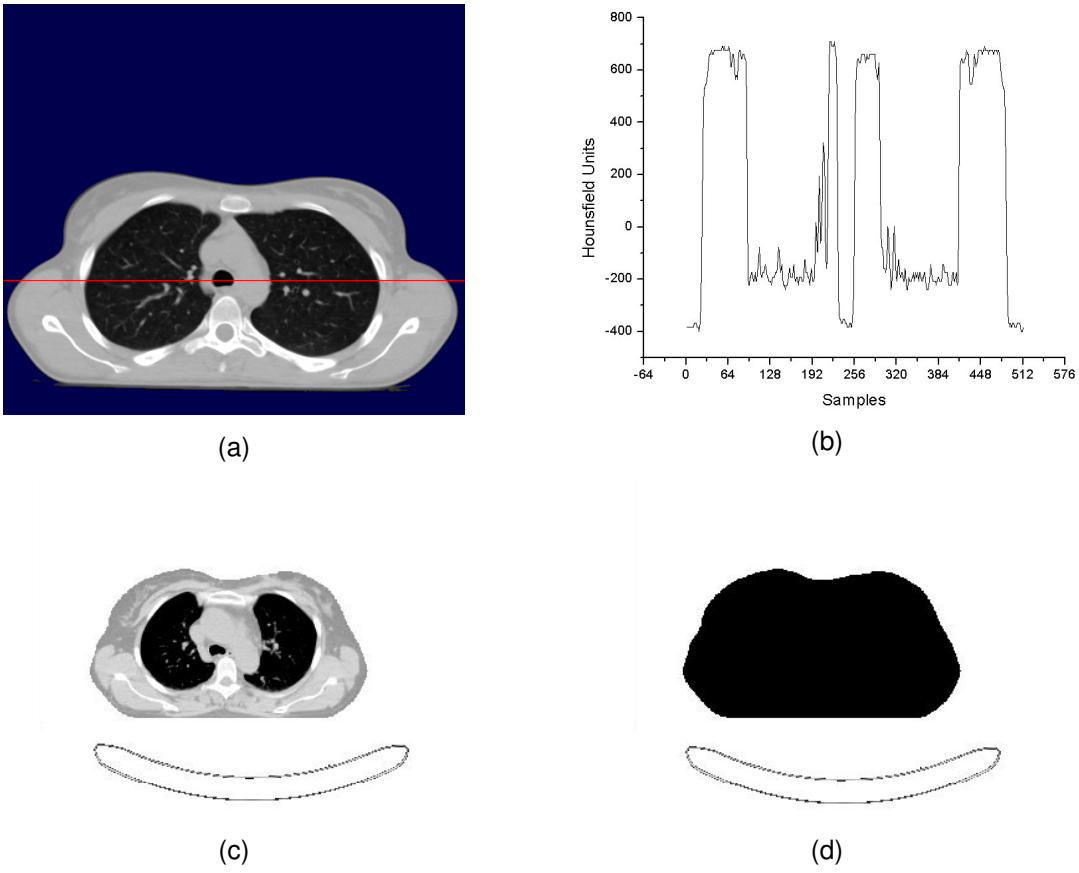

Figure 5-3. Line sampling over an axial CT slice. In (a) the CT slice with the red line indicator. In (b) the sampled valued reconstructed as signal. In (c) filling of the axial CT slice of the chest. In (d) the internal body volume is marked as empty (0).

and its six adjacent voxels is less than a given threshold, pre-classified using a binary LUT, then the current voxel is merged with the growing region. This process is repeated recursively to grow the object until not more voxels can be found.

An example with optimal RG result is presented in Figure 5-3(c) and (d). The seed point used for the RG process has been defined to be the upper left corner of the volume. The background volume and the skin layer have been completely extracted and are illustrated with white colour on the axial CT slices. Regardless of the successful application of the RD algorithm, the RG process might lead to erroneous results. Potential reason for that can be the sensitivity to changes of the acceptance criteria. This means that sub optimal parameter selection will force the region growing algorithm to "overflow" the skin surface boundaries and continue addressing voxels to the auxiliary volume that have similar HU e.g. fat soft tissue. Also discontinue or indistinct tissue boundaries in two or three dimensions are a problem that cannot be handled easily from the region growing method. Usually there is a small "bridge" of voxels that allow the transfer of the seed through them into a region with similar acceptance criteria. The CT data used in this work belong often to patients with disease on the neck region. In this case the error one can observe is the leak of the region growing approach from the room air through the cavity to the respiratory system (e.g. the mouth and the nose) and thus they reach the trachea, which has the same grey values as the room area. When this occurs it is not possible to visualize the shape of the trachea.

Generally speaking, to overcome the above limitations of the RG most researchers combine the method with data filtering and then an edge detection method [Pavlid90], [Masut96]. This edge detection step could provide additional information about the exact location of the region boundaries. Afterwards the region sorting and merging is always profitable. Our main concern is to eliminate bridges of voxels with low grey values, for simplicity we will call the air-voxels. Thus prior to the RG algorithm the edges of the complete grey-value volume are detected calculated and stored in the opacity volume. The edge detection is achieved using the gradient estimator from [Levoy88] since it provides good detection and localization and iso-contour value selectivity. An important feature of this method is that one can adjust the thickness of the boundaries. This allows merging of structure boundaries and closing gaps of air-voxels. This step optimises the object boundaries generating opaque borders. Important for our application is that by manipulation of the gradient estimator voxel "bridges" between structures are eliminated, stopping this way the RG algorithm from leaks. However there might be cases where edge detection is not enough to compensate the leaking error of the RG algorithm for this purpose, manual definition of the region borders must be then defined in means of a bounding box.

5.5 Rendering & RG Results

The reconstruction of 3D images using volume rendering directly from the original data is capable of re-expressing anatomic information with a high degree of realism. This is a great advantage against 3D reconstruction of segmented volumes or surfaces. This advantage is most apparent when visualizing small structures and complicated anatomical sites. The following sessions present the integration of the background volume defined above in the main rendering pipeline.

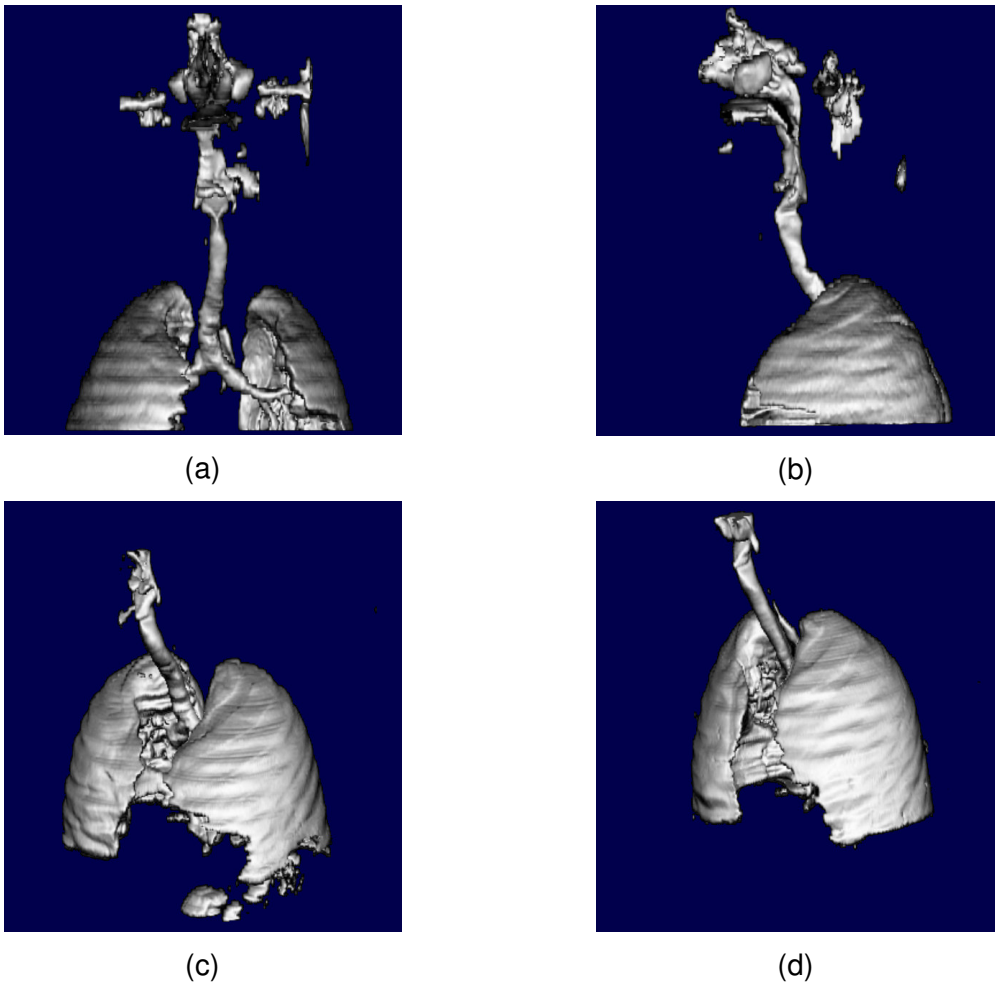

Figure 5-4. Surface reconstruction examples of the airway and lungs volumes on different patient cases. Reconstructions are done using opacity volumes.

5.5.1 Direct Surface Reconstruction

The background volume that has been extracted using the region growing approach will serve to the recalculation of the opacity volumes, gradient contour based and the iso-value region based, in order to obtain clear view of the lung and trachea volume. The opacity calculation employed in this work is based on the research paper from Levoy [Levoy88]. For the calculation of the iso-value contour opacity, the opacity classification procedure assigns an opacity value $\mathbf{a_v}$ to each voxel with value $\mathbf{f_v}$ and an opacity value close to $\mathbf{a_v}$ for those voxels that have a voxel value close to $\mathbf{f_v}$. The rest of the voxels will have zero opacity value. For the iso-value region based the opacity value have binary values: opacity value $\mathbf{a_v}$ to each voxel with value $\mathbf{f_v}$. During opacity volume calculation we incorporate now the background volume estimated above. In this case those voxels that belong to the β_v=1 will receive zero opacity values.

For the surface reconstruction of the lungs and airway a well-established surface visualization method has been used. In addition the opacity volume calculation generates thicker edges due to the principle of the algorithm. As shown previously the edge thick-

ness depends on the radius that will be selected for the opacity volume generation. Since the initial body boundaries are in a closer range than original HU volume boundaries during selective recalculation of opacity with the background volume only some parts of the skin surface will be neglected. The rest of them do not coincide for the background volume and therefore will appear on the final image. This problem can be solved after applying multiple dilations to the background volume, forcing the expansion of the volume size towards the skin surface and main body volume. This opacity volume will be further used for the surface reconstruction of the airway and lungs. The important outcome of these images is the clear visualization of the surface of the lungs and the airway path using the standard volume reconstruction pipeline and only after data pre-processing. At this point the lungs and airway volume have been completely isolated and reformed means of the opacity volume. The opacity volume has been used directly to generate the images illustrated in Figure 5-4. The next paragraph will demonstrate additional advantages of the opacity volume that could be due to its use in combination with the DRR reconstruction

5.5.2 Integration to DRR Reconstruction

The DRR images can be generated using direct volume rendering combined with a transfer function that will assign specific predefined values to the voxels under sampling (see section 2.4). One type of transfer functions allows the user to adjust the HU conversion simulating the physical properties of the tissues. More elaborate techniques can be employed to directly model the physical interactions and simulate the X-ray sources of different energies. In Chapter 2 we demonstrated that using user-defined transfer functions e.g. a triangular transfer function, one can amplify specific voxel values, converting the low attenuation tissues into tissue with high attenuation coefficients. The chest is a challenging region for visualization applications and especially the DRR. This anatomical site is more difficult for investigation than others because bone, soft tissues, as well as the lungs and airway must all be visible with sufficient contrast. The lungs and the airway are tissues that are not clearly visible during visualization of the DRR. In contrast, airway is clearly visible on both traditional radiographs and megavoltage portal images representing an important anatomic landmark.

Previous research works presented a number of methods in order to improve the DRR contrast for those lung and airway structures. These methods involve the use of user defined transfer functions, e.g. a triangular LUT, that one can amplify specific voxel values, converting the low attenuation tissues into tissue with high attenuation coefficients. The final DRR image could contain only the specific tissue type ignoring the rest of the structures. As an extension of this approach presented in [Killo01] the full tissue range DRR and the airway DRR could be “blended” as 2D images into a single image. The images can be combined by addition or one image can be subtracted from the other. However the disadvantages of this process are that two images must be generated, one with full tissue range and a second one including only the airway or lungs. Furthermore the final image is influenced from artifacts that are introduced from the amplified room air values. Therefore initially the user must introduce a volume bounding box region that will include only the volume of interest, excluding large parts of the volume data that contain room air.

An obvious standard for comparison of the DRR result is the traditional radiographs. DRRs and conventional radiographs appear different for several reasons. Among them the most important are image quality in terms of spatial resolution and image contrast. The main limiting factors for the spatial resolution of the final image is the image resolu-

tion as well the spatial resolution of the CT data. Most significant errors are introduced by the slice thickness and the only means to reduce this drawback is to increase the longitudinal resolution of the CT data. Conventional radiographs are generated with lower X-ray energy than that used in CT scanners. It is well known that the tissue attenuation coefficients are directly related to the X-ray energy. Thus attenuation coefficients derived from CT data represent a higher ratio of Compton to photoelectric interactions. In contrast the above drawbacks, CT imaging offers a great advantage on the result image contrast against the conventional radiographs. The image contrast on a slice image is given with direct comparison of the attenuation value of neighbouring volume elements and by the line integrals representing a path through the complete volume. Thus, small differences in the density or the composition of tissues can therefore be rendered with sufficient contrast as a matter of principle. This principle is true for all slice-imaging modalities. Nevertheless, recent studies [Dicks03], [Bolle03] have proven that DRRs quality and mainly accuracy of anatomical representation can be comparable to conventional X-ray films and can replace them through different clinical procedures. This is the case under the condition that DRRs are generated from CT volumes with slice thickness of equal or less than 6mm. Bollet et. al used DRRs, that have been generated using 3mm and 6mm slice thickness, and portal images, for the comparison of the patient position variation between CT planning and treatment phase. DRRs generated from 6mm slice thickness, gave less precision of set-up error evalution.

Based on that principle the generation of DDR images offer by far more features than the realistic radiographs. In this work the proposed two different approaches that extent beyond the standard transfer functions that are based to the physics by which a traditional radiograph is produced. Although this approach is contradictory to the physics of the X-ray radiographs the produced DRR images visualize more anatomical information for the lungs and airway and can be more clinically useful. In both methods a combinatory rendering using the original data values and the pre-calculated opacity volume of the mentioned anatomical structures has been realized. The first approach presents a modified version of the rendering pipeline for the X-ray absorption model. The second method involves a hybrid reconstruction of the X-ray absorption model and the surface illumination model based on the opacity volume.

5.5.2.1 Direct DRR Deconstruction

The physical principle of X-ray attenuation is the basis of DRR rendering. The attenuation process of an X-ray beam traversing a distance ***D*** within a medium is an exponential function, as shown in Eq 5.1

$$I(s) = I_0 \exp(-\int_D \mu(x, E_0)\,\mathrm{dx}) \qquad \text{Eq 5.1}$$

Here ***I(s)*** is the intensity after the X-ray has traversed a distance of ***D*** within the medium, I_0 is the intensity of the incident X-ray, μ is the linear attenuation coefficient and E_0 is the energy for a monochromatic X-ray beam at point x. Eq 5.1

simply states that the intensity of an X-ray beam exiting an object is reduced from the incident intensity of the X-ray according to the linear attenuation coefficient of the

traversed material. The linear attenuation coefficient is closely related to the density of the material as well as the energy of the X-ray beam. In addition, Eq 5.1

can be approximated by the discrete summation form of Eq 5.2:

$$I_s = I_0 \exp(-\sum_{i=1}^{N} \mu_i x) \qquad \text{Eq 5.2}$$

I_s is the X-ray intensity when it arrives at the film. The less intensity of an X-ray reaching the film, the brighter the film is. Considering the X-ray film exposure process, a DRR image represents the negative image of the film rather than the same picture. Therefore, the intensity of one pixel in a DRR image is normalised by the transparency T, see Eq 5.3. The final pixel intensity is then corrected by a gamma correction to simulate the X-ray film exposure process.

$$I_p = I_0 * (1 - T) \qquad \text{Eq 5.3}$$

where $T = \exp(-\Gamma(P_0 P_1))$ is called transparency and $\Gamma(s) = \sum \mu_i \, x$ is the optical length.

In addition, based on Eq 5.2 the main computation cost in DRR volume rendering is to calculate the optical length, $\Gamma(s)$, i.e. the average attenuation coefficient.

$$\Gamma(s) = \frac{L}{N} \sum_{i=1}^{N} \mu_i = L(\frac{1}{N} \sum_{i=1}^{N} \mu_i(E)) \qquad \text{Eq 5.4}$$

where $x = L/N, L = |P_0 P_1|$, N is the number of sampling points when using the equal distance sampling method.

In this work the HU values are categorized in four different tissue types: air, fat, muscles and bones. To reconstruct DRR images with smooth contrast at the tissue boundaries, the tissue attenuation transfer function is generated after linear interpolation between the attenuation coefficients that belong to different tissue types. For each tissue type a weighting index is introduced in order to manipulate their contribution to the final image contrast. For example high index to the bones and low to the soft tissue will result to an image with improved contrast of the bone structures. This approach provides adequate contrast between bones, soft tissues and air. However the definition of “optimal” contrast or “realistic” DRR is somewhat subjective and might vary between different volume data and different observers. The weighted transfer function provides acceptable contrast for bones and soft tissues. The lungs and airway appear with black colour on the DRR image but since the demand for higher contrast for bone and soft tissues dominates the boundaries of the low attenuation structures are not clearly visible.

Most researchers for simplicity during calculations (and in order to produce better results during DRR generation) use the attenuation formula in Eq 5.1. This formula refers to a monochromatic radiation spectrum. However in reality the X-ray radiation spectrum produced from most medical imaging devices that use an X-ray tube is polychromatic. This principle is very often the reason why the X-ray imaging systems, including the CT scanners, may produce artificial structures that deviate from reality. One type of image artifacts that appear in CT images are those caused by the beam hardening effect. Beam hardening is visible in CT images mostly as dark zones or streaks between bone structures and it is caused by preferential attenuation of lower energy photons in polychromatic

radiation. In addition the beam hardening effect depends on the object type and the projection direction. Principally μ_i is a function of the varying mean energies. Thus a specific mass attenuation coefficient e.g. μ_1 will vary with the projection direction since different structures will influence differently the beam attenuation causing fluctuation to beam hardening effect as well. Currently a number of solutions are proposed to eliminate the beam hardening [Yan00], [Elbak02]. The artifacts caused by the beam hardening effect are intensified when metallic implants are present within the volume of the object under scanning. In such cases the image contents might be completely extinguished in the vicinity of the metallic object, leaving only disturbing noise structures. In standard X-ray radiographic imaging modalities the beam hardening effect is especially noticeable in those procedures where "clear" beam energy spectrums are required (e.g. digital mammography). However this problem is more noticeable in the CT imaging as a matter of principle because the back-projection algorithms used for the image reconstruction consider the projection data as being generated using a monochromatic beam spectrum.

By omitting the virtual model of the beam hardening effect when reconstructing the standard DRR images will result to better image contrast since constant values for the attenuation coefficients are used. In this work we will try to simulate the results of the beam hardening effect in terms of linear influence of the beam spectrum during the ray-sampling step. The aim is to produce a better image contrast between the low attenuation structures (lungs-airway) and the surrounding tissues. In order to generalize Eq. 5.2 we assume that the X-ray beam has polychromatic spectrum:

$$I(d) = I_0 \int_E S(E) \exp(-\int_D \mu(x,E)\,\mathrm{dx})\mathrm{dE} \qquad \text{Eq 5.5}$$

Where ***S(E)*** is the beam spectrum profile and satisfies the following properties:

$$S(E) > 0, \ \text{for} \ \forall E \qquad \int_{\mathrm{E}} S(E)dE = 1 \qquad \text{Eq 5.6}$$

A projection ***p(D)*** along a line integral will result to the following equation:

$$p(D) = -\log \frac{I(d)}{I_0} \approx \int_D \int_E S(E)\mu(x,E)\,\mathrm{dE}\,\mathrm{dx} \qquad \text{Eq 5.7}$$

The approximation errors in Eq. 5.4 result in a nonlinear artifacts known as beam hardening in CT imaging. In our projection model we assume that the beam spectrum is composed of two energies E_0 and E_1 that will effect the linear attenuation coefficient function respectively.

$$p(D) = -\log \frac{I(d)}{I_0} \approx \int_D \left(S(E_0)\mu(x,E_0) + S(E_1)\mu(x,E_1)\right)\mathrm{dx} \qquad \text{Eq 5.8}$$

The discrete approximation of Eq 5.4 is given by:

$$I_d = I_0 \exp\left(-\sum_{i=1}^{N} (S(E_0)\mu^0{}_i x + S(E_1)\mu^1{}_i x)\right) \qquad \text{Eq 5.9}$$

The energy E_0 corresponds to the attenuation function $\mu(x,E_0) = \mu_i^0$ the energy E_1 to the $\mu(x,E_1) = \mu_i^1$. Considering Eq 5.6 the relation between $S(E_0)$ and $S(E_1)$ can be expressed as:

$$S(E_0) + S(E_1) = 1 \Rightarrow S(E_1) = 1 - S(E_0) \qquad \text{Eq 5.10}$$

And Eq 5. 7 can be approximated accordingly:

$$I_d = I_0 \exp\left(-\sum_{i=1}^{N} (S(E_0)\mu^0{}_i x + (1 - S(E_0))\mu^1{}_i x) \right) \qquad \text{Eq 5.11}$$

For simplicity the relation between the two attenuation functions could be defined as linear:

$$\mu^1{}_i = \mathrm{w}\mu^0{}_i, \quad w \in [0, 2] \qquad \text{Eq 5.12}$$

The parameter w is user defined. We will name this parameter here attenuation weight. When the $0<w<1$, then the attenuation function μ_i^1 contains reduced values in relation to μ_i^0. If w ranges are $1<w<2$ then the attenuation function μ_i^1 has larger values than the μ_i^0. In case $w = 1$, then both attenuation function have equal values.

The proposed "beam hardening" model depends on the projection direction and the sampling object. The above approach can be easily integrated in the main rendering pipeline. In section 5.5.1 we demonstrate how we can isolate the lung-airway volume using the opacity volume. The same volume will be used during DRR reconstruction so as to activate the "beam hardening" process. Principally as long as the ray traverses voxels that do not belong to the opacity volume, the attenuation weight will be equal to one ($w = 1$), other the weight will obtain the user defined value. The energy spectrum parameter $S(E_0)$ is used with default value 0.5. The following pseudocode presents this principle:

```
SE0 = 0.5;  SumVal = 0.0;
for  i=0 to N (Number of Steps for current ray)
{
      voxel_pos.x = Step_list[i].x;
      voxel_pos.y = Step_list[i].y;
      voxel_pos.z = Step_list[i].y;
      voxel_μi^1 = voxel_μi^0  = μI(TEXTURE_VOLUME(voxel_pos))^0

      if ( OPACITY_VOLUME(voxel_pos) )
      {
            voxel_μi^1 = μI(TEXTURE_VOLUME(voxel_pos))^1
            voxel_μi^0 = μI(TEXTURE_VOLUME(voxel_pos))^0
      }
      voxel_value = SE0* voxel_μi^0 + (1.0 – SE0)  * voxel_μi^1

      SumVal += voxel_value;
}
```

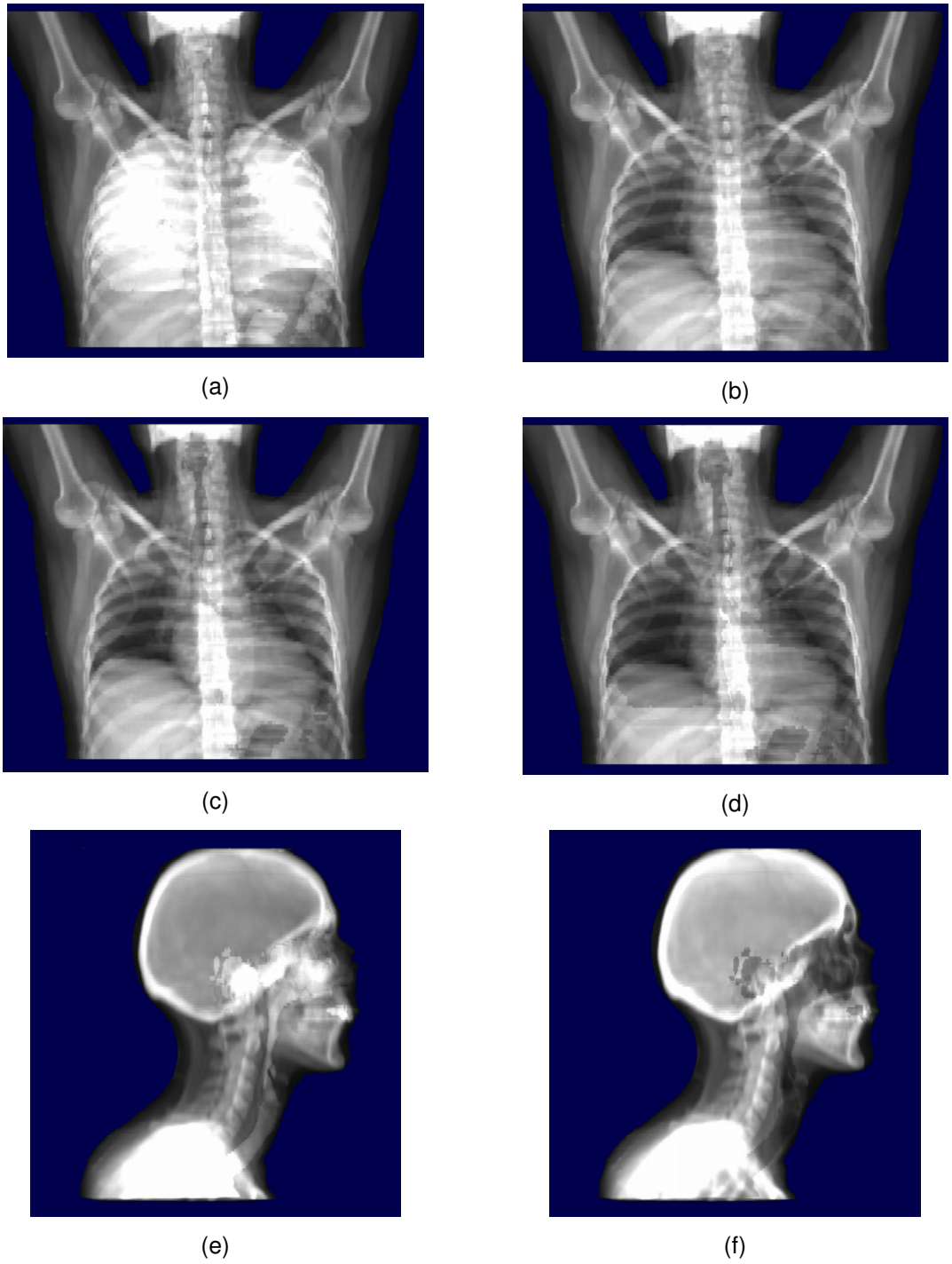

Figure 5-5. Volume reconstruction of CT volumes simulating the beam hardening effect.

The application results of this method are shown in Figure 5-5. Two different CT volumes have been selected: the first from the neck and chest region and the second from the head and neck region. Images (a) and (e) indicate the reconstruction of internal structures with high contrast. This means that the weighting factor in the beam hardening at-

tenuation model takes values greater than one. In the rest of the images Figure 5-5 the internal structures are reconstructed will lower contrast than the surrounding tissues. This indicates weighting values smaller than one.

5.5.2.2 DRR and Direct Surface Rendering Mixing

So far we exploit the possibility of reconstructing the opacity volume of using a single illumination model and by sampling the same volumetric information; the CT values data and their relation to the attenuation coefficients. The results of this approach illustrated the generation of non-physical based DRR images that improve the contrast of tissues with low attenuation. By using an optical model that simulates the X-ray process we generate superimposed images. In such a case that final pixel information is collected under the partial contribution of the specific property of each anatomical structure. Although each structure has a different impact to the sampling process the final result will be always affected from the structure that dominates the ray path quantitatively and qualitatively. In other word structures with small volume and lower contrast will be overlaid from "competitor" structures. In addition depth information will be neglected.

An alternative visualization method could be the reconstruction of both information volumes, CT and opacity volume. In this occasion we have to deal with two different illumination models: the X-ray model and the volume-surface reconstruction model, which is based on standard light shading methods. Data intermixing could be achieved in different levels [CaiSa99]: illumination model level intermixing, accumulation level intermixing and image level intermixing. Considering the two candidates-visualization models one important information is omitted from the DRR model: the depth information. The lack of depth information in the DRR model does not allow the selective distinction between different organ surfaces. As result one cannot apply the volume intermixing steps as this could be done using the surface boundaries of the objects. The following paragraphs describe the approach that has been employed in this work to merge the volumetric information generated using the two different illumination models.

This approach is the simplest and most common used in order to fuse two or more images. The image merging process, similar to the known process of image blending, can be applied on the final images after mixing the pixel intensities of both images. Defining a blending factor $\boldsymbol{w}$, $\boldsymbol{I_T}$ and $\boldsymbol{I_L}$ the corresponding pixel intensities of the DRR image and the surface reconstructed image of the lungs-airway respectively, then the pixel intensity of the result image will be defined as:

$$I_F = Min\left((I_T + \mathrm{w} * I_L), 255.0\right) \qquad \text{Eq 5.13}$$

We consider as focal image the DRR view. Thus we aim to visualize the surface volume within the transparent view of the DRR. The visual effect of Eq. 5.13 is the fade-in and out of the surface volume when the blending factor $\boldsymbol{w}$ is modified interactively. Large w value will intensify the surface image and vice versa. In addition with interactive manipulation of the intensity value in one image e.g. intensity reduction in $\boldsymbol{I_T}$, will result in domination of the intensity values of the final image $\boldsymbol{I_F}$ from the image $\boldsymbol{I_L}$. This effect allows the investigation of structure relationship between the two volumes, DRR and surface, on the projection plane (see Figure 5-6(a) & (b)).

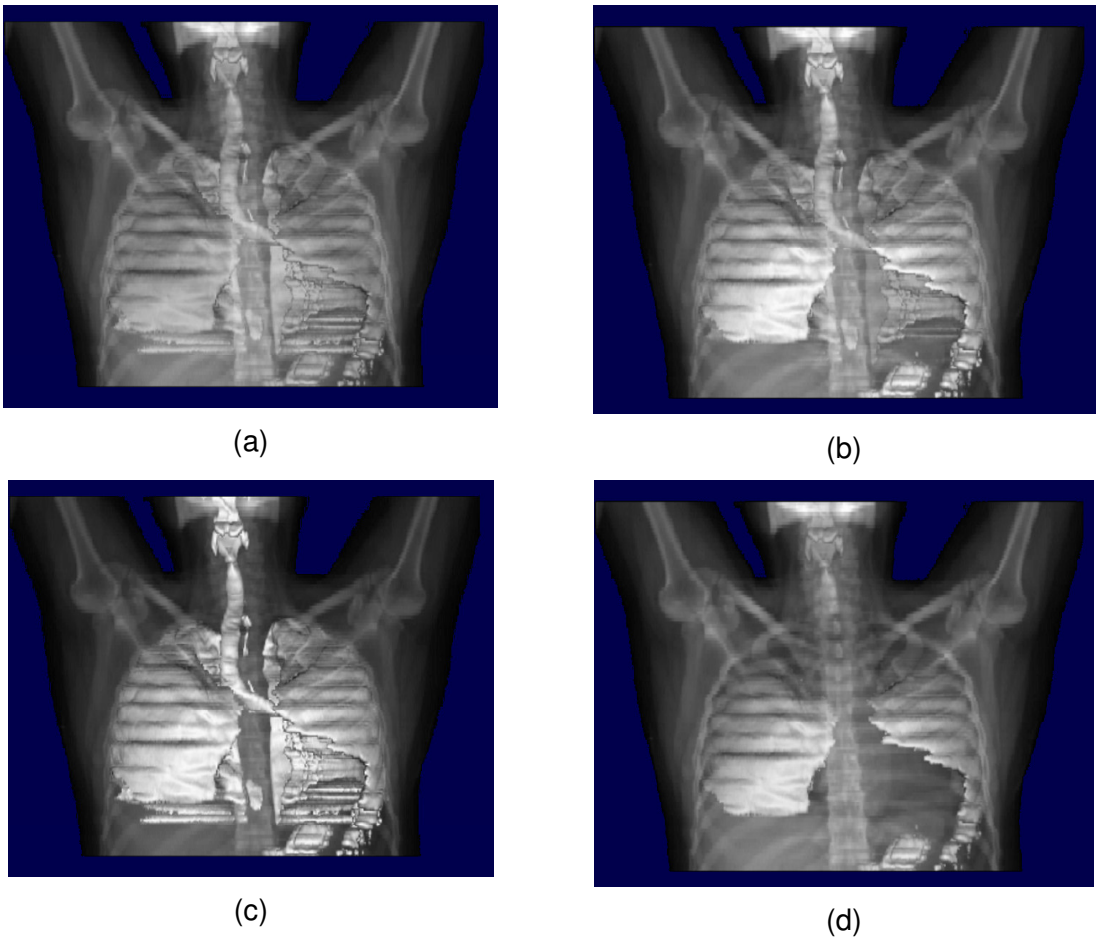

Figure 5-6. Reconstruction of chest DRR and internal structure surface. In images (a) and (b) the DRR and surface information are merged on image level using then image intensity values. In (c) and (d) image intensity values of the surface reconstruction are weighted using the depth information.

An extension of this approach could involve the contribution of the depth information of the surface position. The new image intensity could be defined accordingly:

$$I_F = Max\left((I_T + \mathrm{w} * \mathrm{d_o} * I_L), 255.0\right) \qquad \text{Eq 5.14}$$

Where d_o is the optical depth calculated in relation to the viewing direction:

$$d_o = \sqrt{Max\left(0.0, \left(1.0 - \left(\frac{Z_{Min} - Z_S}{Z_{Min} - Z_{Max}}\right) * w_d\right)\right)} \qquad \text{Eq 5.15}$$

Where $\boldsymbol{Z_{Min}}$, $\boldsymbol{Z_{Max}}$ the minimum and maximum depth value of the viewing box respectively, $\boldsymbol{Z_S}$ the corresponding depth value of the surface for the current pixel and $\boldsymbol{w_d}$ a weighting factor defined and manipulated from the user. The visual effect of Eq. 5.14 is presented in Figure 5-6 (c) & (d). By increasing the weighting factor $\boldsymbol{w_d}$ the deeper re-

gions of the surface volumes in relation to the viewer direction are getting diffused allowing the viewer to screen regions of the transparent image. The advantage of this method is that one can better appreciate the location of the surface volume in depth in relation to the transparent volume when needed. In this application the lung-airway volume has higher priority than the transparent volume.

5.6 Integration into 3D Simulation

In the frame of this work it is important to incorporate conventional generated volume rendered images with into the treatment planning routine. A crucial step of the plan evaluation during radiotherapy planning is the geometric comparison of the field configuration with the defined GTVs and in relation with the rest of the patient anatomy. Standard visualization techniques in radiotherapy use the BEV projection onto the DRR combined with the treatment beam shape and the GTV projection. Such reconstructions assure the tumor coverage during irradiation. As already mentioned standard DRR techniques can effectively display bony and surface/skin anatomy, but they are ineffective for displaying soft tissue anatomy as demonstrated in previous paragraphs (see section 5.3). In this section we demonstrate the integration of the proposed reconstruction method into the CT simulation visuals as part of the treatment planning process. The proposed method is integrated in both available reconstructed mode of the CT Simulation: in the BEV and in the OEV. In both cases the reconstruction pipeline used is the same as in the previous reconstructed results. However for the BEV reconstruction a perspective projection is used in order to simulate conventional X-ray reconstruction.

Figure 5-7 demonstrates a patient with neck carcinoma. In this case the GTV is defined and the spinal canal volume is segmented and marked as organ at risk. Under normal circumstances the standard DRR reconstruction would provide the visual result as shown in Figure 5-7(a). The pharynx and trachea borders can be hardly seen on the rendered image even after contrast manipulation. The volume the isolated soft tissue and air (STA) volumes are illustrated with blue color in order to enhance rendering contrast. The mixing model between all volumes has been done on the image level. The color intensity between the segmented volumes and the STA volume is done considering the depth location of the surface. This depth weight can be adjusted depending on user demand and the pixel intensity of the images is given using the formula:

$$I_F = \begin{cases} w * I_{VOI} + (1.0 - w) * I_{STA}; \text{if } d_{VOI} \le d_{STA} \\ w * I_{STA} + (1.0 - w) * I_{VOI}; \text{if } d_{VOI} > d_{STA} \end{cases} \qquad \text{Eq 5.16}$$

Where $\boldsymbol{w}$, defines the blending factor $\boldsymbol{I_{VOI}}$ and $\boldsymbol{I_{STA}}$ the corresponding pixel intensities of the reconstructed segmented volumes (VOI) image and the STA volume reconstructed image respectively.

The second example illustrates a female patient with breast carcinoma. In this case the target volume is very near the lung volume and the treatment field is crossing part of the right lungs. Using the proposed reconstructed method the lung volume is clearly visible and their project area on the DRR can be easily isolated in contrast to the conventional reconstruction methods. Further more the exposed lung region to the treatment field can be better observed on the OEV image on the surface reconstruction mode rather than on the 2D slices. This is shown in Figure 5-8 where the virtual light field projection is originally overlaid on the patient's skin. The same technique is applied on the isolated lung

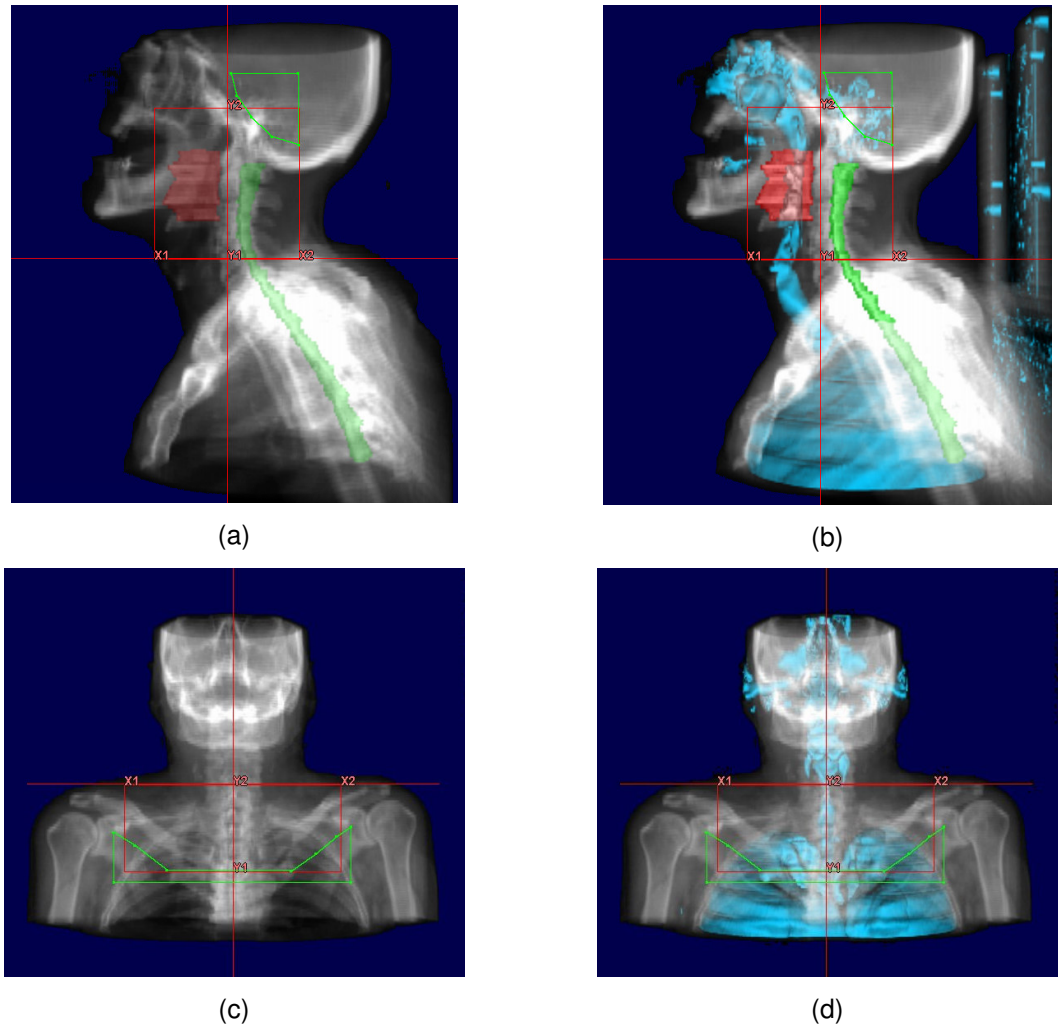

Figure 5-7. BEV reconstruction of a patient with neck carcinoma. On the left image the standard volume rendering techniques are used to render the CT volume and the segmented organs. On the right side the low contrast volume of the trachea and lungs is automatically extracted using the RG methods and rendered using the image blending method. On the lower row the BEV is reconstructed from the anterior view lack of volumes of interest.

volume and the result is shown on the second image. In this case the user can see the lung region exposed on the irradiation field.

So far it has been illustrated that air volumes can be interactively isolated lack of any user adjustments. The only requirement has been to setup the preconditions related to the HU range of lungs and trachea volumes. Nevertheless there are treatment cases where the trachea brunches are covered from the lung volumes and they are not visible when using surface reconstruction modes. To isolate the trachea volume we incorporate the depth buffer in combination with the RG algorithm. The depth buffer refers to the surface depth position relative to the viewer and is found at that point where the ray traversing process ends after hitting the surface of a structure. The information stored at the depth will be immediately the corresponding 2D slice level as a reference of the coordinate point. The user can interactively select from the screen the location of the trachea and the corresponding 3D point will be used as the starting point for the RG algorithm.

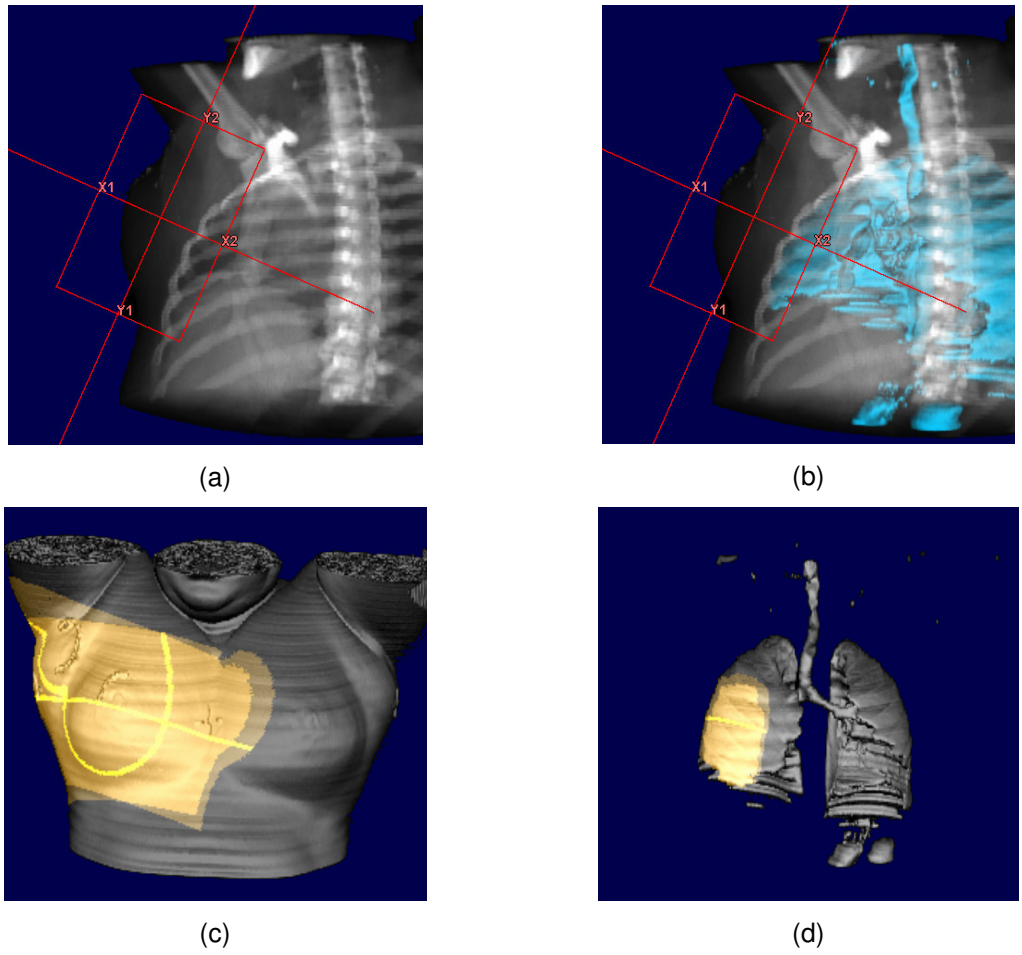

Figure 5-8. OEV reconstruction of a female patient mamma carcinoma. On the top row DRR reconstructions with standard (left) and combined (right) rendering techniques. The lower images indicate the impact of the new method over the virtual light field projection of the treatment beams.

The range of the values used for the volume filling are in the range of –700 to –500 HU and the product of this process will reset every opacity value outside the trachea volume. The results of this process are shown in Figure 5-9 where the organ tissue absorption is manipulated in order to increase contrast of low-density structures during DRR generation. One can notice the weak contrast of the air-way path in Figure 5-9(a). Extraction of the complete air volumes can lead to a mixed image between DRR and surface reconstruction as presented so far, which hints information related to the air way brunching path (see Figure 5-9(b)). A minor modification of our algorithm can trace the air paths until their entrance in the lungs and the contrast achieved is superior to the standard DRR reconstruction techniques Figure 5-9(c).

5.7 Summary

In this chapter we present the utility of volume rendering reconstruction in the frame of the CT based 3D simulator of radiotherapy planning, focusing on the thoracic and neck region. Volumetric surface representation of the critical organs in the above region, such as trachea and lungs, are essential to use as anatomical reference markers and as organs

at risk respectively. In addition we presented how our approach can delineate the airways, especially the trachea bifurcation point, an important landmark for localization and treatment planning. The mentioned anatomical structures must appear with optimum visibility on the reconstructed DRR along the complete 3D simulation process.

The proposed method can be integrated into any rendering pipeline and requires minimized or no user interaction for adjusting the necessary parameters. Taking advantage of the volume rendering techniques that offer high quality visualization, we dramatically reduce user effort required for the segmentation of the previous mentioned anatomical structures. The method can be used to present detailed anatomical structures using the direct volume rending principle that would have been very difficult to reconstruct using standard segmentation techniques.

One of the important components of our approach is the use of a binary volume map in order to address all voxels that belong to the air volume that surrounds the patient's body. This processing step is initialised and completed automatically at the data pre-processing level. Then air volume map is used during ray traversing to reject or accept the sampling voxels. Also, the method can improve the reconstruction of the DRR enhancing the contrast of the subject structures making them applicable for clinical use. By merging both visual information mentioned above we can produce unique images for clinical purpose extending the capabilities of the 3D-Sim process and improving treatment planning outcome. Further more the method could be extended and used for standard diagnostic and volume measurement procedures. Isolating the soft tissue volumes is a process that can be fully automatic without any user intervention. Isolating the trachea volume needs a user starting point selection. The processing time required for soft tissue volume extraction is at the range of half a minute even for volumes with 120 to 150 slices and the 3D reconstruction can be considered as real time on a Pentium III processor of 933 MHz.

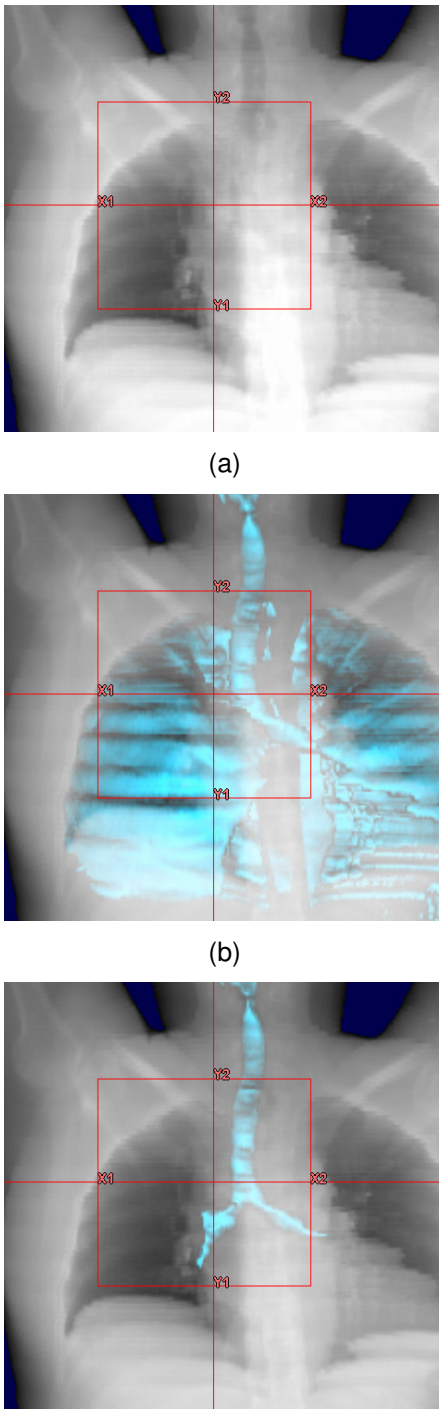

Figure 5-9. DRR reconstruction simulating megavoltage X-ray energy (a). Surface reconstruction of soft tissues (b) and isolation of trachea volume (c)

Finally an extension of this approach could be used for the development of an automatic segmentation of the lung and trachea anatomy.